Original Paper

American Society for Neurochemistry

ASN Neuro
Volume 10: 1–22
© The Author(s) 2018
Article reuse guidelines:
sagepub.com/journals-permissions
DOI: 10.1177/1759091418803282
journals.sagepub.com/home/asn
SAGE

An *In Vitro* Model of Charcot-Marie-Tooth Disease Type 4B2 Provides Insight Into the Roles of MTMR13 and MTMR2 in Schwann Cell Myelination

Danielle C. Robinson[1,2], Anna E. Mammel[1,3], Anne M. Logan[1,2], Aubree A. Larson[1], Eric J. Schmidt[1], Alec F. Condon[1,2], and Fred L. Robinson[1,4]

Abstract

Charcot-Marie-Tooth Disorder Type 4B (CMT4B) is a demyelinating peripheral neuropathy caused by mutations in myotubularin-related (MTMR) proteins 2, 13, or 5 (CMT4B1/2/3), which regulate phosphoinositide turnover and endosomal trafficking. Although mouse models of CMT4B2 exist, an *in vitro* model would make possible pharmacological and reverse genetic experiments needed to clarify the role of MTMR13 in myelination. We have generated such a model using Schwann cell-dorsal root ganglion (SC-DRG) explants from *Mtmr13*$^{-/-}$ mice. Myelin sheaths in mutant cultures contain outfoldings highly reminiscent of those observed in the nerves of *Mtmr13*$^{-/-}$ mice and CMT4B2 patients. *Mtmr13*$^{-/-}$ SC-DRG explants also contain reduced Mtmr2, further supporting a role of Mtmr13 in stabilizing Mtmr2. Elevated PI(3,5)P_2 has been implicated as a cause of myelin outfoldings in *Mtmr2*$^{-/-}$ models. In contrast, the role of elevated PI3P or PI(3,5)P_2 in promoting outfoldings in *Mtmr13*$^{-/-}$ models is unclear. We found that over-expression of MTMR2 in *Mtmr13*$^{-/-}$ SC-DRGs moderately reduced the prevalence of myelin outfoldings. Thus, a manipulation predicted to lower PI3P and PI(3,5)P_2 partially suppressed the phenotype caused by Mtmr13 deficiency. We also explored the relationship between CMT4B2-like myelin outfoldings and kinases that produce PI3P and PI(3,5)P_2 by analyzing nerve pathology in mice lacking both Mtmr13 and one of two specific PI 3-kinases. Intriguingly, the loss of vacuolar protein sorting 34 or PI3K-C2β in *Mtmr13*$^{-/-}$ mice had no impact on the prevalence of myelin outfoldings. In aggregate, our findings suggest that the MTMR13 scaffold protein likely has critical functions other than stabilizing MTMR2 to achieve an adequate level of PI 3-phosphatase activity.

Keywords

myelination, Schwann cell, myotubularin, endosomal trafficking, phosphatidylinositide 3-kinase, phosphatidylinositide 3-phosphatase

Received April 24, 2018; Received revised August 7, 2018; Accepted for publication August 9, 2018

Introduction

Myelin is a multilamellar, spiral wrapping of specialized plasma membrane which glial cells elaborate in order to ensheath axons (Nave and Werner, 2014; Salzer, 2015). Schwann cells and oligodendrocytes are the specialized glia that generate myelin in the peripheral and central nervous systems, respectively. By localizing sodium channels to Nodes of Ranvier and by optimizing the electrical properties of the axolemma, myelin makes possible rapid, saltatory nerve impulse conduction (Rasband and Peles, 2015). Myelin membranes are rich in lipids but also

[1]Department of Neurology, Jungers Center for Neurosciences Research, Oregon Health & Science University, Portland, OR, USA
[2]Neuroscience Graduate Program, Oregon Health & Science University, Portland, OR, USA
[3]Cell, Developmental & Cancer Biology Graduate Program, Oregon Health & Science University, Portland, OR, USA
[4]Vollum Institute, Oregon Health & Science University, Portland, OR, USA

Corresponding Author:
Fred L. Robinson, Department of Neurology, Jungers Center for Neurosciences Research, Oregon Health & Science University, Mail Code L623, Portland, OR 97239, USA.
Email: robinsof@ohsu.edu

Creative Commons Non Commercial CC BY-NC: This article is distributed under the terms of the Creative Commons Attribution-NonCommercial 4.0 License (http://www.creativecommons.org/licenses/by-nc/4.0/) which permits non-commercial use, reproduction and distribution of the work without further permission provided the original work is attributed as specified on the SAGE and Open Access pages (https://us.sagepub.com/en-us/nam/open-access-at-sage).

contain very high levels of a few key myelin-specific proteins (Nave and Werner, 2014). Myelinating glia also provide trophic support, notably by exchanging metabolites with axons through specific transporters or gap junctions (Balice-Gordon et al., 1998; Nave and Werner, 2014; Kleopa and Sargiannidou, 2015). Extensive signaling interactions between axons and Schwann cells govern nerve development, myelination, the nerve's response to injury, axonal regeneration, and remyelination (Monk et al., 2015; Salzer, 2015). Diseases of myelin, such as peripheral neuropathy, leukodystrophy, and multiple sclerosis, represent a significant disease burden for which there are few effective treatments (Pouwels et al., 2014; Brennan et al., 2015; McMurran et al., 2016).

Charcot-Marie-Tooth disease (CMT) is a group of phenotypically heterogeneous disorders which affect peripheral nerves (Jerath and Shy, 2015). With a prevalence of about 1 in 2,500, CMT is one the most common inherited neurological disorders (Skre, 1974). CMT-causing mutations have been identified in about 80 genes (Baets et al., 2014; Fridman and Reilly, 2015; Jerath and Shy, 2015). Electrophysiology and other clinical criteria can be used to differentiate between the axonal and demyelinating forms of CMT, which can broadly be viewed as initially affecting either the axon or the Schwann cell, respectively (Scherer and Wrabetz, 2008). In demyelinating CMT, secondary axonal loss is the best correlate of clinical severity (Krajewski et al., 2000).

Proteins mutated in demyelinating CMT regulate a number of different Schwann cell processes and are, in some cases, myelin structural proteins. However, nearly half the human proteins linked to demyelinating CMT are believed to regulate membrane traffic within the endosomal-lysosomal pathway (Brennan et al., 2015). *DNM2,* factor-induced gene 4 (*FIG4*), FGD1-related F-actin-binding protein (*FRABIN*), lipopolysaccharide-induced tumor necrosis factor-alpha factor (*LITAF*)/*SIMPLE,* myotubularin-related 2 *(MTMR2*), *MTMR5, MTMR13,* and SH3 domain and tetratricopeptide repeats 2 (*SH3TC2*) are broadly expressed in human tissues, yet patients bearing mutations in these genes are largely spared from phenotypic deficits other than peripheral neuropathy. These observations suggest that myelinating Schwann cells are particularly vulnerable to disturbances in endosomal trafficking; the reason for this vulnerability is unclear.

CMT4B is a severe subtype of demyelinating CMT which results from mutations in myotubularin PI (phosphoinositide or phosphatidylinositol) 3-phosphatases (MTMR2, MTMR5, and MTMR13; Figure 1) (Bolino et al., 2000; Senderek et al., 2003; Nakhro et al., 2013). The condition is characterized by childhood onset, severe axon loss, segmental demyelination or remyelination, and the presence of distinctive myelin outfoldings, which are thought to arise from excessive longitudinal growth of myelin (Previtali et al., 2007; Vaccari et al., 2011). Myotubularin phosphatases selectively remove a phosphate from the third position of phosphatidylinositol 3-phosphate and 3,5-bisphosphate (PI3P and PI(3,5)P_2, respectively), two lipids that regulate membrane traffic through the endosomal-lysosomal network by recruiting specific effector proteins from the cytosol (Figure 1; Taylor et al., 2000; Walker et al., 2001; Schink et al., 2016).

The mechanism by which the loss of MTMR2 or MTMR13 causes abnormal myelination remains poorly understood. The selective elimination of *Mtmr2* from Schwann cells was demonstrated sufficient to trigger the formation of CMT4B-like myelin outfoldings in mice (Bolis et al., 2005). Given that MTMR2 and MTMR13 likely function as a complex which dephosphorylates PI3P or PI(3,5)P_2, it is predicted that these two substrates are elevated when either member is absent; elevated levels of PI3P/PI(3,5)P_2 may disturb endosomal trafficking and signaling (Figure 1). Indeed, it has been plausibly suggested that elevated PI(3,5)P_2 is at the basis of myelin outfolding formation in *Mtmr2*-deficient Schwann cells (Vaccari et al., 2011). Unlike MTMR2, MTMR13 is a catalytically inactive phosphatase that functions as a scaffold protein; MTMR13 binds to MTMR2 and other endosomal proteins and also activates Rab guanosine triphosphate (hydrolases) (GTPases; Robinson and Dixon, 2005; Jean et al., 2012; Figure 1). In the context of myelination, the relative importance of MTMR13's potential function as a regulator of phosphoinositides or as an activator of Rab GTPases has yet to be determined.

Although mouse models of CMT4B2 (MTMR13-deficiency) have been established and have yielded insights (Tersar et al., 2007; Robinson et al., 2008), an *in vitro* model of this dysmyelinating condition would be useful for investigating the aforementioned mechanistic aspects of MTMR13 function. Here, we describe the generation and characterization of such a model. We also provide insight into the relationships between MTMR13, MTMR2, and the phosphoinositide substrates of the phosphatase complex.

Materials and Methods

Lentivirus Production

Third-generation lentiviruses were produced using a published method (Tiscornia et al., 2006). Viral packaging was accomplished by transfecting 293FT cells (Invitogen) with a transfer vector and the packaging plasmids pREV, pVSVG, and pMDL, which encode Rev, the envelope protein VSVG, and Gag-Pol, respectively (Tiscornia et al., 2006). To concentrate lentiviral particles, virus-laden supernatants were filtered and

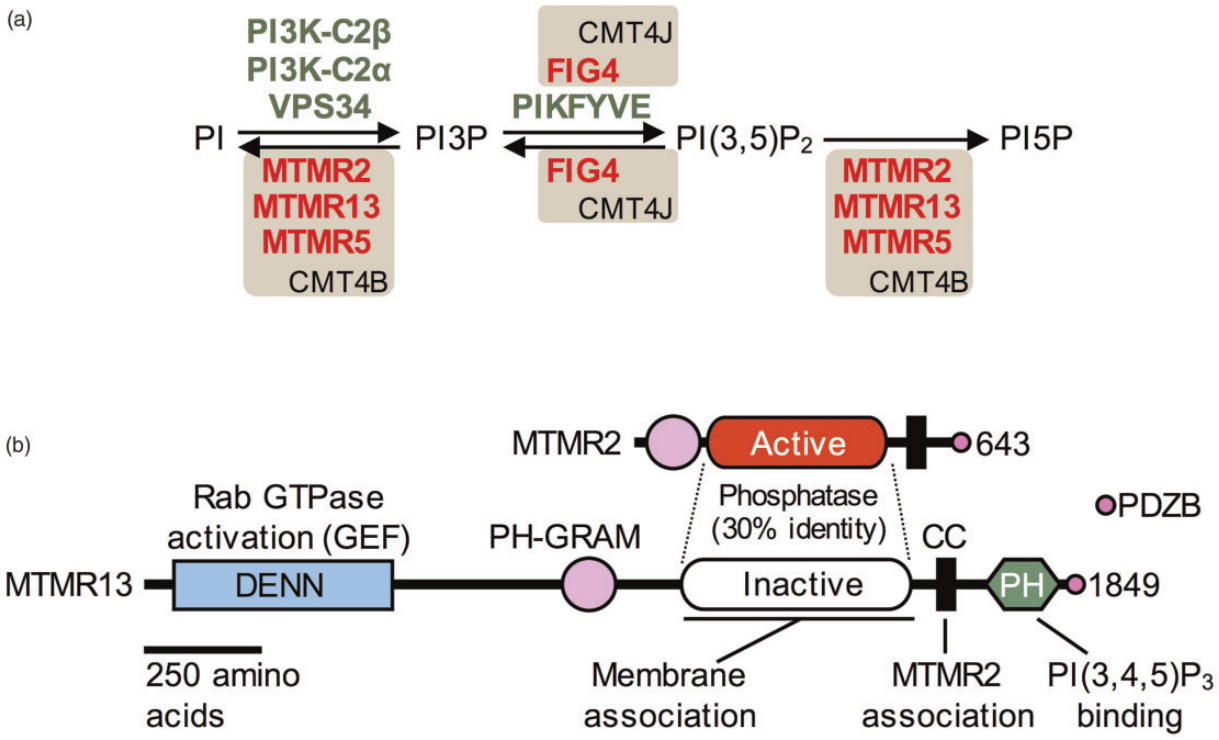

Figure 1. (a) Enzymatic pathway thought to be responsible for the production of the majority of PI3P in mammalian cells and for the further metabolism of PI3P. PI kinases and PI phosphatases are indicated in green and red, respectively. Recessive mutations in specific PI phosphatases (tan boxes) have been shown to cause the indicated forms of demyelinating CMT. In mammalian cells, the predominant function of the PI3P 5-phosphatase FIG4 is thought to be the stimulation of PIKFYVE kinase activity, although the enzyme is capable of dephosphorylating PI(3,5)P_2. (b) Protein domains or motifs present in MTMR2 and MTMR13 as well as the understood functions of specific sequences. MTMR2 contains a PI 3-phosphatase domain specific for PI3P and PI(3,5)P_2; MTMR13 contains a pseudophosphatase domain which lacks enzymatic activity. Coiled-coil (CC) sequences in both MTMR2 and MTMR13 are required for association of the two proteins. PDZB = PDZ (domain)-binding; MTMR = myotubularin-related; DENN = differentially expressed in normal versus neoplastic; GEF = guanine nucleotide Exchange Factor; PH = Pleckstrin homology; GRAM = glucosyltransferases, Rab-like GTPase activators and myotubularins.

subjected to ultracentrifugation (83,000 × *g*; 2 h; 4°C; Beckman Coulter SW 41 Ti rotor). Pelleted viral particles were resuspended in sterile phosphate-buffered saline (PBS) with 1% bovine serum albumin (BSA), and stored at −80°C. Lentiviral titers were determined by flow cytometry for enhanced green fluorescent protein (EGFP) expression in transduced 293FT cells. Serial dilutions of a concentrated lentiviral stock were prepared and used to transduce 293FT cells (in triplicate). Forty-eight hours after transduction, cells were trypsinized and resuspended in PBS. EGFP expression was analyzed using a Guava easyCyte Flow Cytometer (Millipore). GuavaSoft™ (Millipore) and FlowJo (v9.9.6) softwares were used to determine the percentage of cells expressing EGFP. Titers for lentiviral stocks were reported as titer units/ml (TU/ml) and used to achieve specific multiplicities of infection (MOIs).

The lentiviral transfer vector, lentivirus phosphoglycerate kinase GFP (LVPG) was a generous gift from Gregory Dissen. In LVPG (7,630 bp), the cytomegalovirus (CMV) promoter in the backbone vector p156RRLsinPPT (Follenzi et al., 2000) is replaced with a 519-bp human phosphoglycerate kinase (PGK) promoter. LVPG contains (5′ to 3′) a Rous sarcoma virus (RSV) promoter-5′LTR (R-U5) sequence, a Rev responsive element (RRE), a central polypyrimidine tract (cPPT), a PGK promoter, an EGFP open reading frame (ORF), a woodchuck hepatitis virus posttranscriptional regulatory element, and a self-inactivating 3′LTR (ΔU3-R-U5). The LVPG-EGFP-MTMR2 transfer vector was constructed using standard polymerase chain reaction (PCR)-based DNA cloning methods; all manipulated portions of the vector were confirmed correct by DNA sequencing. The 239 amino acid EGFP protein sequence encoded by LVPG is identical to that encoded by EGFP-C1 (GenBank Accession U55763.1). The protein linker sequence between EGFP and MTMR2 in LVPG-EGFP-MTMR2 is SGLRS. The human MTMR2 protein encoded by LVPG-EGFP-MTMR2 is identical to the reference sequence

(GenBank Accession NP_057240.3) except for the presence of a previously reported common MTMR2 polymorphism (Lys_3 to Thr; Bolino et al., 2001; Houlden et al., 2001). The ORF for the EGFP-MTMR2 fusion protein resides between the *XbaI* (5′) and *SalI* (3′) restriction endonuclease sites of LVPG.

Myelinating Explant Cultures From Dorsal Root Ganglia

Wild-type (C57BL/6) or *Mtmr13*$^{-/-}$ female mice (N8 generation on C57BL/6) were bred to males of their same genotype, respectively. At 13.5 days of gestation, pregnant females were killed, and embryos were removed and placed in Dulbecco's phosphate-buffered saline (DPBS; Life Technologies) on ice. Each litter of embryos was held in DPBS, while the individual embryos were sequentially dissected. To isolate E13.5 dorsal root ganglia (DRG), embryos were individually removed from DPBS and placed for gross dissection in a 6-cm glass Petri dish containing 2 ml of 37°C Leibovitz's L-15 medium (Life Technologies) supplemented with 10% fetal bovine serum (FBS) and 0.5% penicillin-streptomycin (P-S; 50 units/ml of penicillin and 50 μg/ml of streptomycin). The trunk of the embryo was isolated and transferred to a new 60-mm glass Petri dish (lined with Sylgard-184 silicone) containing 2 ml of 37°C L-15 medium (10% FBS, 0.5% P-S), for spinal cord isolation. The spinal cord (with attached DRG) was dissected from the vertebral column using fine forceps and transferred to a new Sylgard-184-lined glass Petri dish (60 mm) containing 2 ml of 37°C L-15 medium (10% FBS, 0.5% P-S). Individual DRGs were plucked off with Dumont #5 forceps. DRGs were then removed from the dissection dish and transferred, using a 200-μl micropipette, to a 14-ml conical tube containing 7 ml of L-15 medium (10% FBS. 0.5% P-S). This conical tube was held in a 37°C water bath in between dissections of embryos. All of the DRGs dissected from the embryos of a given pregnant female were pooled.

All subsequent DRG culture procedures were carried out in a biological safety cabinet; all media were prewarmed to 37°C. When the dissections were complete, the volume was adjusted to 14 ml by adding 7 ml of L-15 medium (10% FBS, 0.5% P-S). DRGs were allowed to settle in the conical tube for 10 to 20 min in a 37°C water bath. All but ~0.5 ml of the medium was carefully removed and 14 ml of L-15 medium lacking serum and P-S was added back to the tube. DRGs were again allowed to settle for 10 min in a 37°C water bath. All but ~0.5 ml of the medium was carefully removed and 5 ml of Trypsin-ethylenediaminetetraacetic acid (EDTA; 0.25%; Invitrogen) was added. The DRGs were then incubated in a 37°C water bath for 45 min. Five milliliters of L-15 medium (10% FBS, 0.5% P-S) was added, and the DRGs were pelleted by centrifugation for 30 s at $170 \times g$. The pelleted DRGs were washed once in 10 ml of 37°C L-15 medium (10% FBS, 0.5% P-S) and again centrifuged at $170 \times g$ for 10 min. The medium was removed and replaced with 2 ml of 37°C M1 medium (Modified Eagles Medium [MEM]; Life Technologies; 5.2 g/L D-glucose; 10% FBS) containing mouse nerve growth factor (NGF 2.5S Native Mouse Protein; Life Technologies) at 50 or 10 ng/ml.

DRGs were triturated by aggressively pipetting up and down 10 times using a 200-μL micropipette. Triturated isolates were centrifuged for 5 min at $170 \times g$ and subsequently resuspended in 1 ml of M1-NGF medium. Cells were counted using a hemocytometer. Dissociated DRGs were plated at the density of 130,000 total cells per well by placing a 160-μl drop of the cell suspension in the center of a 25-mm circular coverslip that had been coated with a solution of rat tail collagen (0.5 mg/ml). Using a fine pipette tip on a 20-μL micropipette, three bubbles were introduced at the center of the drop of suspended cells (to encourage the cells to adhere in the center of the coverslip). Cultures were incubated overnight at 37°C in 5% CO_2.

The day on which embryos were dissected was designated culture Day 0. On culture Day 1, 1 ml of M1-NGF medium was added to each well of explant culture. On Days 3, 5, and 7, the medium was replaced with a fresh 2 ml of M1-NGF medium. On Day 8, the medium was changed to 2 ml of C medium (MEM; Life Technologies, 10% FBS, 29 mM D-glucose, and 3.76 mM L-glutamine), which contained 50 μg/ml ascorbic acid (AA) to promote myelination by endogenous Schwann cells, and 50 or 10 ng/ml NGF. On Days 11, 14, 17, and 20, the medium was replaced with 2 ml of fresh C medium (with AA and NGF). On Day 21, cultures were either fixed for immunofluorescence or lysed for immunoblotting.

When Schwann cell-dorsal root ganglion (SC-DRG) cultures were infected with lentiviruses, the culture protocol was identical to that described earlier except as follows: On Day 5, the fresh M1-NGF medium contained the appropriate amount of lentiviral particles needed to achieve the desired MOI. On Day 6, the virus-containing medium was removed, the explant was washed twice with C medium containing NGF, and 2 ml of C medium with NGF was added. On Day 7, no action was taken. We found that an MOI of 15 to 20 was the lowest amount of virus which routinely yielded Schwann cell transduction rates of 90% or greater. To assess the rate of lentiviral transduction, all of the Schwann cells in four or five 100 μm^2 60× Z-stack images were visualized with 4′,6-diamidino-2-phenylindole (DAPI) and scored as positive or negative for EGFP fluorescence in the associated Schwann cell body.

Immunofluorescence

After 21 days in culture, DRG explants were washed once with PBS and fixed in 4% paraformaldehyde (PFA) in PBS (pH 7.4) for 15 min at room temperature (RT) on a rocking platform. Fixed cultures were washed three times with PBS and subsequently permeabilized in ice-cold methanol for 5 min (on ice). After washing once with PBS, cultures were blocked for 1 h in PBS containing 10% normal goat serum (NGS). Fixed cells were covered with a solution of PBS with 0.1% Tween-20 (PBST), which contained 2% NGS and appropriately diluted primary antibodies; this mixture was incubated overnight at 4°C on a rocking platform. Primary antibodies used for immunofluorescence were a rat anti-myelin basic protein (MBP) monoclonal antibody (mAb; Millipore Cat# MAB386 RRID:AB_94975), and a chicken anti-neurofilament H polyclonal antibody (pAb; IgY fraction; Abcam Cat# ab4680 RRID:AB_304560). After an overnight incubation at 4°C, cultures were washed 3 times for 10 min with PBST. Fluorescent secondary antibodies (Jackson ImmunoResearch) were diluted to 3 μg/ml in PBST containing 2% NGS and applied to cultures. Cultures were then incubated for 1 h at RT on a rocking platform. After incubation with secondary antibodies, cultures were washed thrice for 10 min with PBST. Cell nuclei were labeled with 0.36 μM DAPI, via a 1-min RT incubation. Cultures (on coverslips) were next washed twice for 5 min with PBST, rinsed once in distilled deionized (dd) water, and mounted on ColorFrost™ Plus microscope slides (ThermoFisher) using Elvanol as a mounting medium. When SC-DRG cultures were infected with lentiviruses expressing EGFP or EGFP-MTMR2, secondary antibodies used were Cy3-goat-anti-rat (Jackson ImmunoResearch Labs Cat# 112-165-143 RRID:AB_2338250) and AlexaFluor-647-goat-anti-chicken IgY (Jackson ImmunoResearch Labs Cat# 103-605-155 RRID:AB_2337392).

Image Acquisition and Analysis

Images were acquired using a Nikon or Yokogawa CSU-W1 spinning disk microscope, 60× (Nikon Plan Apo VC OFN 25, 1.4, oil) or 40× (Nikon Plan Fluor, 40×, 1.3, oil) objectives, and NIS-Elements AR imaging software (Nikon, V. 4.20.01 build 982). Thirty-six 20-μm Z-stacks (sampled every 1 μm) were randomly selected by programing the microscope to acquire a 6 by 6 grid of images. The 6 by 6 grid was positioned over the explant such that one corner of the grid was set just inside the outer edge of the myelinated portion of the explant. The midpoint of each Z-stack was set by manual focusing. Z-stack images were separated by 1 mm across the grid. With the 60× objective, the field of view for each image was 277.33×234.00 μm. Thus, each coverslip was randomly sampled across a total area of 2.33 mm^2. With the 40× objective, the field of view for each image was 416×351 μm. Thus, each coverslip was randomly sampled across a total area of 5.26 mm^2. Using the Fiji image processing package for ImageJ (v2.0.0-rc-46/1.50 g), Z-stack images were projected into a single image view using the standard deviation of each pixel. Such Z-stacks were used for myelin analysis. The total number of complete myelin segments in each projection was counted, and this number was used to determine the density of myelinated segments (per mm^2) within a given explant. A myelinated segment was included in the analysis only if the full myelin internode was clearly present in the image. The length of myelin segments was measured using Fiji.

To determine the percentage of myelin segments that contained outfoldings, we analyzed only segments for which the full myelin internode was clearly present in the image. We classified a myelin irregularity as an outfolding if the structure met one or more the following criteria: (a) A single, bubble-like structure having a diameter of at least half than that of the myelin sheath to which it is attached, (b) a multilobed, bubble-like structure in which the individual lobes have a diameter of at least half than that of the myelin sheath to which they are attached, (c) a "lollipop"-like structure in which one or two MBP-positive myelin bulbs are connected to the associated myelin sheath by a thin "stalk" (Figure 3(e')), and (d) a cluster of small myelin bubbles (Figure 3(h)). Using these criteria and the explant sampling imaging method described earlier, we determined the fraction of myelinated segments which contained one or more myelin outfoldings. All immunofluorescence-based quantifications of myelin density or the prevalence of myelin outfoldings were carried out with the investigator blinded to the genotype or the treatment being tested.

Electron Microscopic Analysis

Myelinating DRG explant cultures were established and maintained as described earlier. On Day 15 or 21, cultures were fixed in freshly prepared 2% PFA and 1.5% glutaraldehyde in PBS (pH 7.4) overnight at 4°C. Cultures were rinsed with PBS, and a cell scraper was used to dislodge the culture from the coverslip and transfer it to a 1.5-ml tube containing 1 ml of 6% BSA in PBS (pH 7.4). After an overnight incubation at 4°C, cultures were pelleted via centrifugation at $94 \times g$ for 5 min at RT. All but 500 μl of the BSA–PBS solution was removed, and 500 μl of electron microscopy (EM) fixative (1.5% glutaraldehyde, 1.5% PFA, 0.05 M sucrose, 0.25% $CaCl_2$, and 0.1 M sodium cacodylate; pH 7.4) was added to the tube. Samples were incubated at 4°C for at least 4 h to allow the BSA–PBS fixative solution to polymerize. The pelleted cultures, now surrounded in

a gel, were removed, divided into smaller pieces for further processing, rinsed with 0.1 M sodium cacodylate buffer (with 0.05 M sucrose and 0.25% $CaCl_2$; pH 7.4), and further fixed in EM fixative. The samples were then loaded into individual wells of a Ted Pella PELCO Prep-Eze 12- or 6-well specimen holder (containing 0.1 M cacodylate buffer) for microwave-assisted postfixation, dehydration, and embedding. The specimen holder was placed in a 50-mm Petri dish and loaded into the vacuum chamber of a PELCO Biowave Pro 36500 microwave (Ted Pella). Briefly, samples were washed in 0.1 M sodium cacodylate buffer (pH 7.4), postfixed in 2% buffered OsO4, stained *en bloc* with 1% uranyl acetate, dehydrated in graded ethanol solutions (50%–100%), and finally embedded in epoxy resin. Ultrathin (60–90 nm) sections were cut, placed on 200 mesh transmission electron microscopy (TEM) grids and contrasted further with uranyl acetate and lead citrate. Sections were examined using an FEI Tecnai 12 transmission EM operating at 80 kV. Digital images were acquired using a 16-megapixel Advanced Microscopy Techniques XR16M camera. For EM on sciatic nerves, mice were perfused with EM fixative (above); nerves were dissected and processed similarly as described earlier. For light microscopic analysis of sciatic nerves, mice were perfused with EM fixative (above); nerves were dissected and processed similarly as described earlier, except that 500-nm cross-sections were stained with toluidine blue prior to microscopy.

Immunoblotting

To prepare protein extracts, myelinating SC-DRG explants (grown on 25-mm coverslips in six well dishes) were washed once with 2 ml of PBS at RT and placed on ice. The explant material was collected in 200 μL of ice-cold lysis buffer (50 mM Tris [pH 8.0], 120 mM NaCl, 0.5% Triton X-100, 100 mM NaF, 1 mM Na_2VO_4, and 2 mM EDTA) in which one cOmplete™ mini, EDTA-free protease inhibitor cocktail tablet (Roche) was dissolved for every 10 ml of buffer and subsequently homogenized. Extracts were clarified by centrifugation ($15{,}000 \times g$ for 15 min at 4°C), and protein concentrations were determined using Bradford assays. Clarified extracts were prepared for sodium dodecyl sulfate-polyacrylamide gel electrophoresis (SDS-PAGE) by adding NuPAGE LDS sample buffer (Thermo Fisher Scientific) and 1 mM DTT, and heating the sample. The protein (20–25 μg) was resolved in each lane of a NuPAGE 4% to 12% Bis-Tris gel (Invitrogen) and transferred to a polyvinylidene difluoride membrane. A total protein stain (MemCode, Thermo Fisher Scientific) was used to confirm uniform electroblotting transfer of proteins to membranes. Immunoblotting was accomplished by standard methods; immunoblots were quantitated using peroxidase-activated chemiluminescence on a G:BOX Chemi imaging system with GeneSys software (Syngene). After normalization for differences in β-tubulin content, data were normalized such that the mean value for the wild-type sample was either 100 or 1. Primary antibodies used for immunoblotting were mouse-anti-GFP (mAb; UC Davis/NIH NeuroMab Facility Cat# N86/8 RRID: AB_2313651) mouse-anti-ß-tubulin (mAb; clone E7; Developmental Studies Hybridoma Bank, University of Iowa; DSHB Cat# E7 also AB_2315513 RRID: AB_528499). The anti-MTMR2 (119-AN) and anti-MTMR13 (116-AN) rabbit antibodies have been described elsewhere (Robinson and Dixon, 2005; Ng et al., 2013).

Statistics

Graphpad Prism software was used for statistical analyses. Unless otherwise stated in the figure legend, an unpaired t test was used to evaluate significance ($p \leq .05$). Welch's correction was applied to t tests when unequal variance was observed. For SC-DRG explant experiments, $n = 3$ to 7 explants or coverslips derived from 2 to 4 independent (pregnant) female mice for each genotype or treatment. Sample sizes for experiments were based on pilot data, expected or minimum effect size, expected or observed variance, and power analyses.

RNA Expression Analysis

The BioGPS gene annotation portal (www.biogps.org) was used to assess whether the human mRNAs for the endosomal-lysosomal trafficking-linked demyelinating CMT proteins dynamin 2 (*DNM2*), *FIG4, FRABIN, LITAF*/small integral membrane protein of the lysosome/late endosome (*SIMPLE*), *MTMR2, MTMR5, MTMR13*, and *SH3TC2* show broad or restricted expression in human tissues.

Mice

All work with animals was approved by and conformed to the standards of the Oregon Health and Science University Institutional Animal Care and Use Committee. C57BL/6 mice were obtained from Charles River. Vps34 Schwann cell knockout ($Vps34^{SCKO}$) and $Mtmr13^{-/-}$ mice have been described previously (Robinson et al., 2008; Ng et al., 2013; Logan et al., 2017).

Generation of $Pik3c2\beta^{-/-}$ and $Mtmr13^{-/-}Pik3c2\beta^{-/-}$ mice.

$Pik3c2\beta^{+/fl}$ mice (Harada et al., 2005) were obtained from the Jackson Laboratory (Strain: B6.129-Pik3c2btm1Pkha/J). To generate a *null* allele of PI3K-C2β, $Pik3c2\beta^{+/flox}$ mice were crossed with *CMV-Cre* mice (Jackson Laboratory strain B6.C-Tg[CMV-cre]

1Cgn/J). The resulting *CMV-Cre*$^{+}$; *Pik3c2β*$^{+/flox}$ progeny were crossed with C57BL/6 mice to accomplish germ line deletion of *floxed Pik3c2β* exons 3–5. *Pik3c2β*$^{+/\Delta}$ progeny were intercrossed to generate *Pik3c2β*$^{\Delta/\Delta}$ mice, which were subsequently crossed with *Mtmr13*$^{-/-}$ mice (N8 on C57BL/6) to yield *Pik3C2β*$^{+/\Delta}$ *Mtmr13*$^{+/-}$ double heterozygotes, which were then intercrossed to generate *Pik3c2β*$^{\Delta/\Delta}$ *Mtmr13*$^{-/-}$ mice. A three-primer PCR using oligonucleotides EJS-003 (GGCACACACTAACC ACAGCACC), EJS-004 (TCGATGCACGTCTC TCCGC), and EJS-005 (ACACTGGGGTGAGCTGA GCTAGG) was used to genotype mice for *Pik3c2β*. Using these primers, the wild-type, *floxed*, and deleted (Δ) alleles of *Pik3c2β* yield PCR products of 568, 618, and 404 bp, respectively.

Results

Efficient In Vitro *Myelination by Schwann Cells Lacking Mtmr13*

Mtmr13$^{-/-}$ mice have been shown to be a useful model of CMT4B2; these animals recapitulate many key characteristics of the human disease. First, *Mtmr13*$^{-/-}$ mice display the distinctive myelin outfoldings that are a hallmark of CMT4B (Tersar et al., 2007; Robinson et al., 2008). These animals also show reduced nerve conduction velocity, consistent with a demyelinating form of peripheral neuropathy (Tersar et al., 2007; Robinson et al., 2008). Finally, aged *Mtmr13*$^{-/-}$ mice show marked axonal loss, hypomyelination, and evidence of demyelination or remyelination (Ng et al., 2013), all characteristics of CMT4B2 (Previtali et al., 2007). In summary, *Mtmr13*$^{-/-}$ mice effectively model both the initial dysmyelination and subsequent segmental demyelination of CMT4B2, as well as the advanced axonal pathology of the human condition. We sought to determine if *Mtmr13*$^{-/-}$ mice could be used to generate an *in vitro* model of CMT4B2 dysmyelination. Such a model would make feasible the reverse genetic and pharmacological experiments that are needed to clarify the function of the enigmatic MTMR13 pseudophosphatase (reviewed in Raess et al., 2017).

Elegant experimental methods for studying *in vitro* myelination by rodent Schwann cells were developed in the late 1980s (Eldridge et al., 1987) and have since been used to study a number of aspects of myelination and Schwann cell–axon interactions (Maurel et al., 2007; Bolis et al., 2009; Lewallen et al., 2011). Using adaptations of such methods, we established dissociated SC-DRG explant cultures from wild-type and *Mtmr13*$^{-/-}$ mice at embryonic (E) Day 13.5. In culture, dissociated DRG sensory neurons elaborate new axons, which are subsequently myelinated by Schwann cell precursors present in the explanted material (Eldridge et al., 1987). Immunofluorescence microscopy of neurofilament H and MBP was used to visualize axons and compact myelin, respectively, in SC-DRG explants after 21 days in culture. We also established a semiautomated microscopy imaging method that allowed for an unbiased sampling of a large portion of the explant area, which was typically about 15 mm in diameter (Figure 2(a) to (c)). This method was used to quantitate myelin segments, thereby providing an assessment of the efficiency of myelination. As segmental demyelination is a feature of CMT4B2, we assessed the capacity of *Mtmr13*$^{-/-}$ Schwann cells for myelination *in vitro*. The extent of myelination was similar in wild-type and *Mtmr13*$^{-/-}$ explant cultures (Fig. 2A-D). Robust myelination in *Mtmr13*$^{-/-}$ explant cultures is consistent with the observation that myelin is of normal thickness in young adult *Mtmr13*$^{-/-}$ mice (Tersar et al., 2007; Robinson et al., 2008).

An In Vitro *Model of CMT4B2 Dysmyelination*

A hallmark of CMT4B is the presence of myelin outfoldings (Ohnishi et al., 1989; Quattrone et al., 1996; Othmane et al., 1999; Previtali et al., 2007). When viewed in transverse sections, such structures appear as redundant loops of myelin flanking the primary myelin sheath (Previtali et al., 2007). In mutant mouse nerves, CMT4B-like myelin outfoldings appear to preferentially arise from regions of noncompact myelin (paranodes and Schmidt-Lanterman incisures; Bolino et al., 2004; Tersar et al., 2007; Robinson et al., 2008); these structures are thought to result from excessive longitudinal growth of myelin membranes (Vaccari et al., 2011). Schwann cell-specific deletion of *Mtmr2* has been shown to be sufficient to provoke myelin outfoldings in mice; loss of Mtmr2 in motor neurons does not trigger outfoldings (Bolis et al., 2005). The underlying etiology of CMT4B-type myelin outfoldings is unclear. It has been suggested that formation may involve abnormal endosomal-lysosomal myelin membrane trafficking in regions of noncompact myelin, a change that may lead to increased incorporation of membrane-bearing vesicles into myelin sheets (Bolis et al., 2009).

The morphology of nonmyelinating, Remak bundle Schwann cells is normal in *Mtmr13*$^{-/-}$ mice (Robinson et al., 2008), suggesting that Mtmr13 may only be essential when Schwann cells generate myelin. The compaction and the periodicity of peripheral myelin in *Mtmr13*$^{-/-}$ mice has also been demonstrated to be normal (Robinson et al., 2008). Intriguingly, MTMR13 is expressed in many other cells types throughout the human body, including those of the central nervous system. Despite this, CMT4B2 patients (and *Mtmr13*$^{-/-}$ mice) appear to be spared from phenotypic deficiencies other than demyelinating peripheral neuropathy. The

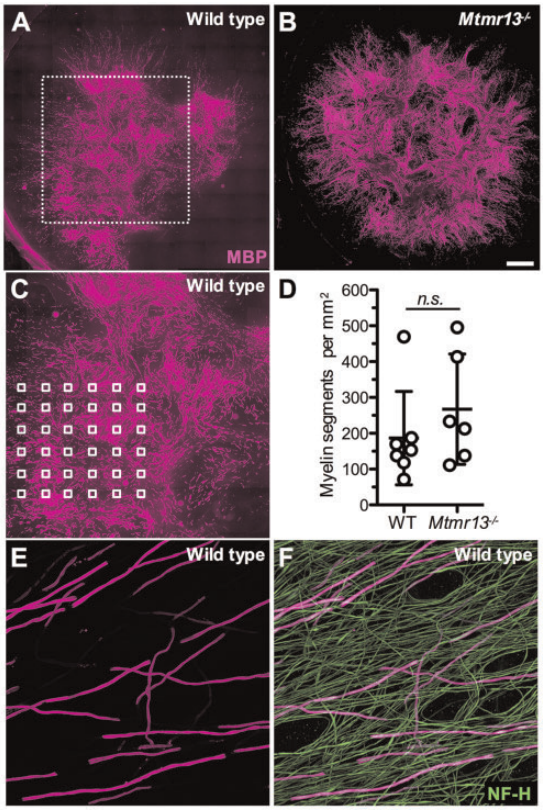

Figure 2. Robust *in vitro* myelination in DRG explant cultures from Mtmr13-deficient mice analyzed using a semiautomated image collection method. Dissociated DRG explant cultures were generated from wild-type and *Mtmr13*$^{-/-}$ embryos at E13.5 and cultured for 21 days under conditions that promote myelination. Myelin and axons were visualized via immunofluorescence with antibodies to myelin basic protein (MBP; *magenta*) and neurofilament heavy chain (NFH; *green*), respectively. (a and b) Low-magnification images of full SC-DRG explants from wild-type and *Mtmr13*$^{-/-}$ mice show qualitatively similar extents of myelination. The overall shapes of explants vary considerably without respect to genotype. (c) A magnification of the indicated portion of (a), overlaid with a grid indicating the area sampled via the automated acquisition a set of 36 high-magnification images. The outermost corner of the grid was positioned at the outer edge of the myelinated explant. (d) Similar density of MBP-positive myelinated segments in SC-DRG explants from wild-type and *Mtmr13*$^{-/-}$ mice. Myelin density: 186.6 ± 130.2 versus 267.3 ± 153.9 MBP-positive segments per mm^2 for wild type and *Mtmr13*$^{-/-}$, respectively; $p = .2949$; Mann–Whitney test; mean ± *SD*; $n = 7$ and 6 independent explants for wild type and *Mtmr13*$^{-/-}$, respectively. In assessing myelin density, an average of 1,067 myelin segments were counted per explant/coverslip (the median value was 806 myelin segments counted per explant/coverslip). (e and f) An example of a high-magnification image corresponding to one of the 36 images derived from the grid depicted in (c). Quantification of myelin segments was accomplished via analysis of images such as that shown in (e). The color white indicates the overlap of green and magenta in (f). Scale bar: 2 mm (a and b), 1.13 mm (c), 20 μm (e and f). MTMR = myotubularin-related.

sole apparent exception to this observation is that most CMT4B2 patients are also diagnosed with early-onset glaucoma (Kiwaki et al., 2000; Azzedine et al., 2003; Hirano et al., 2004). In aggregate, the data suggest that the absence of MTMR13 triggers a defect in myelin sheet structural homeostasis. This defect is likely present during initial postnatal myelination in mice and results in the steady accumulation and growth of myelin outfoldings as mice mature and age (Ng et al., 2013). Eventually, ill-defined abnormalities in MTMR13-deficient Schwann cells lead to segmental demyelination (Kiwaki et al., 2000; Azzedine et al., 2003; Senderek et al., 2003; Hirano et al., 2004; Ng et al., 2013).

Previous work has demonstrated that myelin outfoldings are present in the nerves of *Mtmr13*$^{-/-}$ mice as early as P3, indicating that these abnormal structures form during initial myelination (Ng et al., 2013). To assess whether similar myelin structures form *in vitro,* we examined myelin segments in wild-type and *Mtmr13*$^{-/-}$ SC-DRG explants using immunofluorescence for MBP. We found that myelin segments in *Mtmr13*$^{-/-}$ explants contained MBP-positive protuberances reminiscent of the outfoldings observed in the nerves of *Mtmr13*$^{-/-}$ mice and CMT4B2 patients (Figure 3(b'), (c) to (F'); Othmane et al., 1999; Kiwaki et al., 2000; Azzedine et al., 2003; Senderek et al., 2003; Previtali et al., 2007; Tersar et al., 2007; Robinson et al., 2008).

Myelin outfoldings typically had a nodular appearance, often first projecting away from the myelin sheath, then turning and extending along the longitudinal axis of the internode (Figure 3(b') to (D')). Many myelin outfoldings manifested as elaborate groups of small myelin "bubbles," highly reminiscent of what has been observed in longitudinally sectioned axons in nerve biopsies from CMT4B patients (Ohnishi et al., 1989; Gabreels-Festen et al., 1990; Quattrone et al., 1996; Houlden et al., 2001; Previtali et al., 2007). Broadly speaking, the outfoldings observed by light microscopy in mutant SC-DRG explants project away from the myelin sheath more significantly than the corresponding structures observed in intact *Mtmr13*$^{-/-}$ mouse nerves (Tersar et al., 2007; Robinson et al., 2008; Figure 3(e')). This finding may be a consequence of the crowded environment of the intact nerve, relative to that of the *in vitro* explant culture. Myelin outfoldings in *Mtmr13*$^{-/-}$ explants were observed throughout the internode, including directly adjacent to the Schwann cell nucleus and at the ends of myelinated segments (nodes or heminodes; Figure 3(f') and (h)).

The explant sampling imaging method described earlier was used to assess the prevalence of myelin outfoldings in cultures. We found that myelin outfoldings occurred at a significantly higher rate in *Mtmr13*$^{-/-}$ SC-DRG explants than in wild-type explants (Figure 3 (k)). Although myelin abnormalities that fit our strict

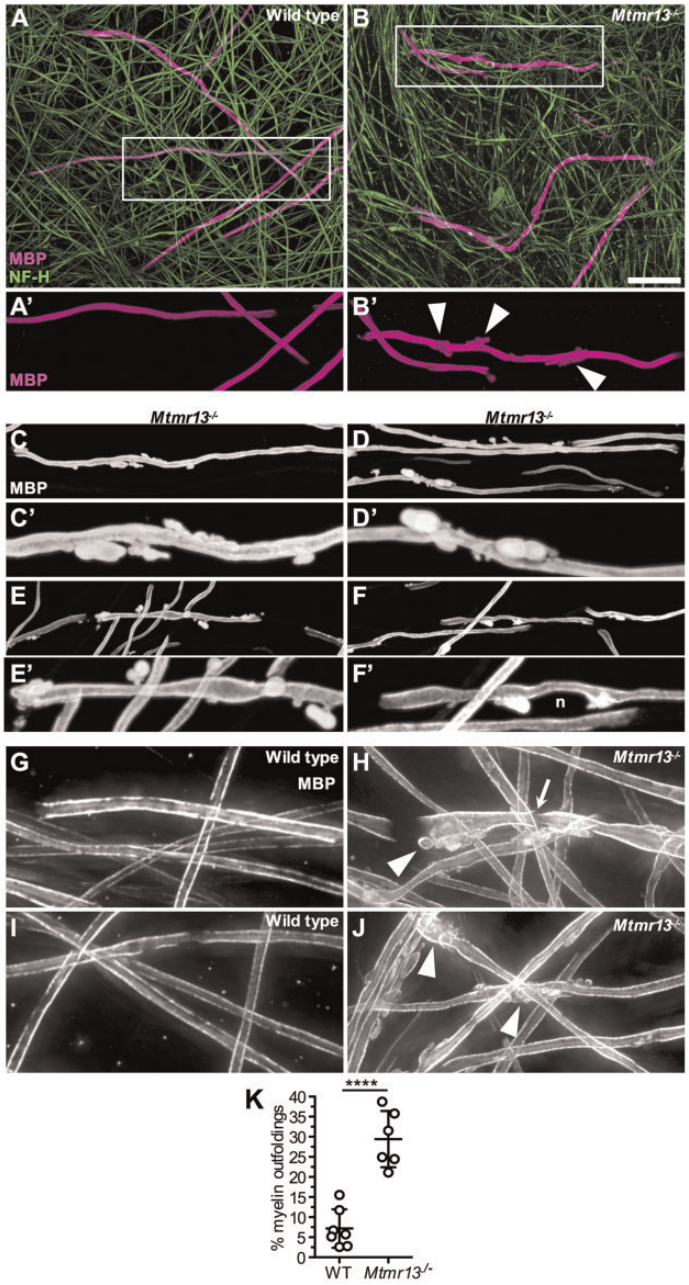

Figure 3. *In vitro* myelination by *Mtmr13*$^{-/-}$ DRG explant cultures leads to CMT4B2-like myelin outfoldings. (a and b) DRG explant cultures from wild-type and *Mtmr13*$^{-/-}$ embryos were analyzed by immunofluorescence after 21 days in culture. Compact myelin and axons were visualized with antibodies to MBP (*magenta*) and NFH (*green*), respectively. Elaborate myelin outfoldings are present in *Mtmr13*$^{-/-}$ cultures but are not observed in wild-type cultures. See "Materials and Methods" section for operational definition of a myelin outfolding. (a' and b') Higher magnification images of the indicated portions of (a) and (b) reveal myelin outfoldings (*white arrowheads*) in *Mtmr13*$^{-/-}$ DRG explant cultures. (c–f) Examples of myelinated segments in *Mtmr13*$^{-/-}$ DRG cultures reveal varying morphologies of outfoldings. (c'–f') Higher magnification images of portions of (c–f), respectively. The location of a Schwann cell nucleus (*n*) is indicated in (f'). (g–j) Deconvolution microscopy of wild-type and *Mtmr13*$^{-/-}$ DRG explant cultures better reveal elaborate, convoluted nature of *Mtmr13*$^{-/-}$ myelin outfoldings (*white arrowheads*), including those at the ends of myelin segments (nodes or heminodes; (h)). A white arrow in (h) indicates a Schmidt–Lanterman incisure. Scale bar: 27 μm (a and b), 17 μm (a' and b'), 24 μm (c, d, e, and f), 8.5 μm (c', d', e', and f'), 8.2 μm (g–j). (k) Quantification of myelin outfoldings in wild-type and *Mtmr13*$^{-/-}$ DRG explant cultures. Percentage of myelin segments containing one or more myelin outfoldings: 7.168 ± 4.784% for wild-type versus 29.42 ± 7.000% for *Mtmr13*$^{-/-}$; mean ± *SD*; ****$p < .0001$; $n = 7$ and 6 explants for wild type and *Mtmr13*$^{-/-}$, respectively. An average of 1,067 myelinated segments per explant were evaluated for the presence of myelin outfoldings (the median value was 806 myelin segments evaluated per explant/coverslip).
MTMR = myotubularin-related.

criteria for classification as outfoldings were present in wild-type cultures, these were significantly smaller and less elaborate than those observed in mutant cultures (see Materials and Methods section).

We also used EM to examine the ultrastructure of myelin formed *in vitro* by mutant Schwann cells. Myelin outfoldings in *Mtmr13*$^{-/-}$ explants were similar in appearance to those found in intact sciatic nerves from mutant mice (Figure 4(a) to (d)). Redundant loops of myelin, although appearing unconnected to the primary myelin sheath when viewed in EM cross sections, are instead likely to be contiguous with the primary myelin sheath, particularly when considered in parallel with MBP immunofluorescence of SC-DRG cultures (Figure 3). The compaction of myelin in *Mtmr13*$^{-/-}$ explants appeared similar to that in wild-type explants (Figure 4 (e) and (f)).

Reduced Mtmr2 Protein in the Absence of Mtmr13 In Vitro

To further explore how SC-DRG cultures from *Mtmr13*$^{-/-}$ mice may recapitulate aspects of the *in vivo* model, we assessed the status of an important binding partner, Mtmr2. MTMR phosphatases comprise a large subgroup of the protein tyrosine phosphatase (PTP) superfamily, which consists of about 105 distinct proteins in humans (Alonso et al., 2004; Tonks, 2013). With 14 MTMR phosphatases identified in the human genome, it is intriguing that such a significant fraction of the PTP superfamily appears dedicated to the dephosphorylation of PI3P and PI(3,5)P_2. Moreover, the fact that nearly half of the human MTMR phosphatases are catalytically inactive indicates important nonenzymatic roles for some members of this protein family. Partially explaining

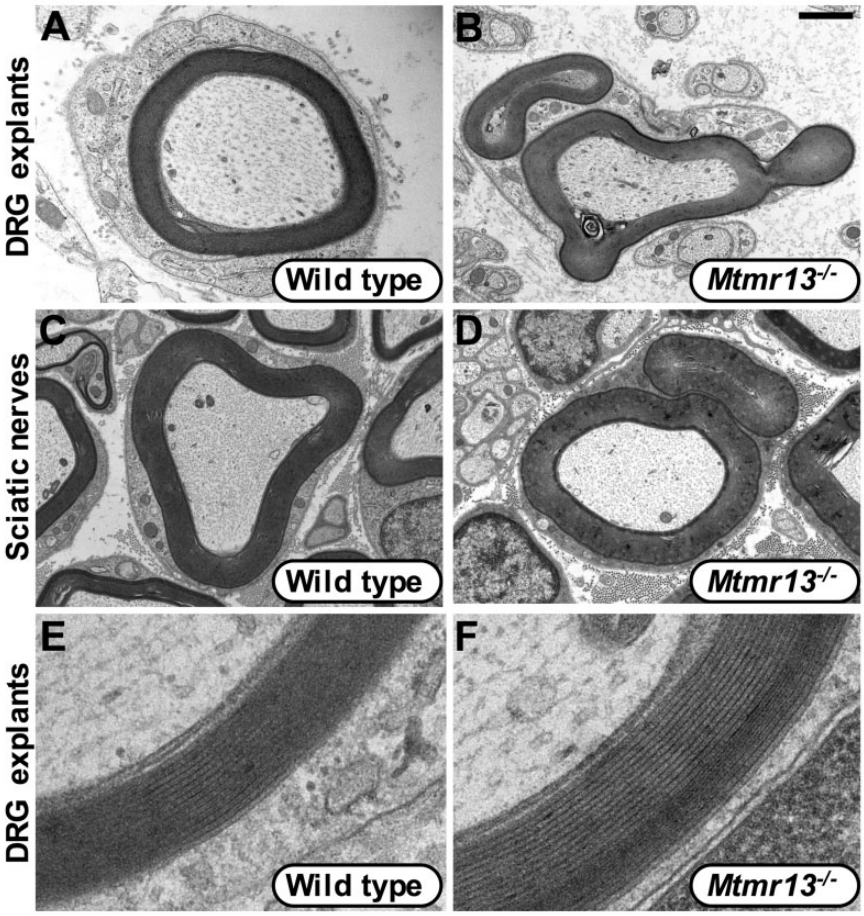

Figure 4. Ultrastructural analysis of myelinated axons in DRG explant cultures and intact sciatic nerves. (a and b) Cross-sections of myelinated axons from wild-type and *Mtmr13*$^{-/-}$ DRG explants analyzed by EM after 15 days in culture. In (b), the mutant Schwann cell contains a redundant loop of myelin, as well as one or two other apparently abnormal myelin protrusions away from the primary sheath. Myelin outfoldings were not observed in wild-type DRG explants examined by EM. (c and d) EM analysis of intact, midsciatic nerves from wild-type and *Mtmr13*$^{-/-}$ mice analyzed at P21 and P18, respectively. A myelin outfolding is observed in the *Mtmr13*$^{-/-}$ nerve (d). (e and f) The compaction of myelin in *Mtmr13*$^{-/-}$ DRG explants was indistinguishable from that observed in wild-type explants. Scale bar: 500 nm (a), 1 μm (b), 1.4 μm (c and d), 128 nm (e), and 102 nm (f). MTMR = myotubularin-related; DRG = dorsal root ganglion.

this latter observation, homo- and hetero-oligomerization among MTMR proteins appears to be an important mode by which this family of phosphatases and pseudophosphatases is regulated (reviewed in Raess et al., 2017). Particularly intriguing is the case of MTMR2, MTMR13, and MTMR5, as the homozygous loss of any one of these three proteins triggers CMT4B, with the condition's distinctive myelin outfoldings (Bolino et al., 2000; Azzedine et al., 2003; Senderek et al., 2003; Nakhro et al., 2013; Figure 1). MTMR2 has been demonstrated to associate with both MTMR13 and MTMR5, in a manner that requires coiled-coil interaction motifs located in each of the proteins (Kim et al., 2003; Robinson and Dixon, 2005; Berger et al., 2006). The association of MTMR2 and MTMR13 is likely to be relevant to CMT4B, as the loss of Mtmr13 significantly reduces the abundance of Mtmr2 in mouse sciatic nerves, indicating a role of Mtmr13 in stabilizing its catalytically active binding partner (Ng et al., 2013).

Consistent with observations in intact mouse nerves, we found that Mtmr2 protein levels were reduced by 35% in myelinating *Mtmr13*$^{-/-}$ SC-DRG cultures (Figure 5). A 35% decrease in Mtmr2 levels may be consequential, particularly if one considers that myelinating Schwann cells are a relatively minor component of the total cellular material in a cultured DRG explant, which contains many nonmyelinating Schwann cells, as well as axons, neuronal soma, and fibroblasts. If the stabilization of Mtmr2 by Mtmr13 only occurs in Schwann cells (or perhaps only in myelinating Schwann cells), the dependence of Mtmr2 on Mtmr13 may be more significant than our quantitation indicates. It has been demonstrated that Mtmr13 is not required for Mtmr2 stabilization in mouse brain tissue or fibroblasts, suggesting that dependence on Mtmr13 is unique to the CMT4B2-relevant sciatic nerve (Ng et al., 2013). Thus, in addition to showing the hallmark myelin abnormality of CMT4B2, explant cultures from *Mtmr13*$^{-/-}$ mice also recapitulate an important biochemical feature observed in mouse nerves, namely, reduced Mtmr2 abundance.

Relationship Between Mtmr13 and Mtmr2 in the Context of Myelination

With an *in vitro* model of CMT4B2 dysmyelination available, we considered whether the outfolding phenotype might be modified by manipulating Mtmr2. As mentioned earlier, Mtmr13 has been shown to bind to and stabilize Mtmr2 (Ng et al., 2013). MTMR13 has also been shown to be largely membrane associated, with the protein's pseudophosphatase domain being sufficient for this localization (Robinson and Dixon, 2005; Figure 1). In myelinating Schwann cells, endogenous Mtmr13 has been demonstrated to be present on endomembrane structures (Ng et al., 2013), which may be endosomes, given that PI3P, a substrate of the MTMR2-MTMR13 complex, is enriched on such membranes. Consistently, investigations of the *Drosophila* orthologs of Mtmr2 and Mtmr13 have indicated that the Mtmr13-like pseudophosphatase functions to recruit

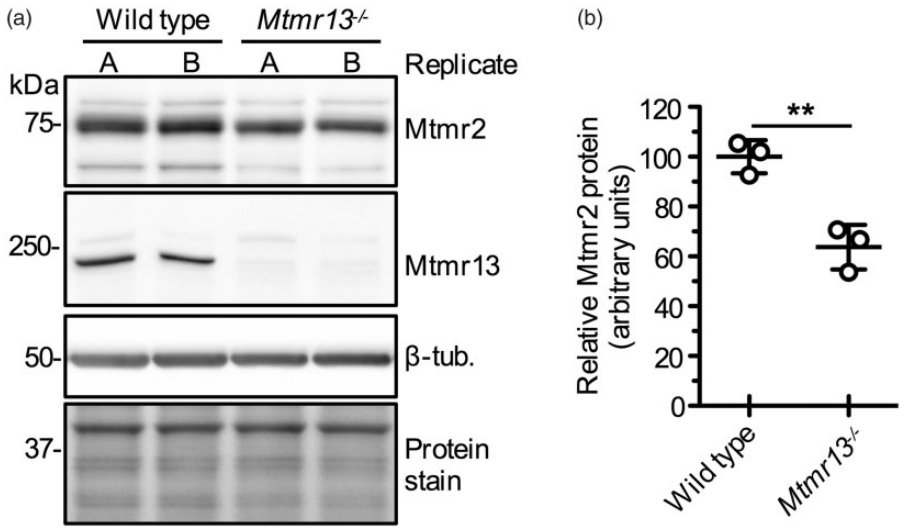

Figure 5. Decreased abundance of Mtmr2 in myelinating *Mtmr13*$^{-/-}$ SC-DRG explants. (a) After 21 days in culture, protein extracts were prepared from SC-DRG explants and analyzed by immunoblotting (25 μg of protein per lane). For either genotype, gel lanes A and B denote replicate explants. (b) Quantitation of relative Mtmr2 protein levels in SC-DRG explants. Mtmr2 protein: 100.0 ± 6.605 for wild type versus 63.70 ± 8.901 for *Mtmr13*$^{-/-}$, respectively (arbitrary units); $n = 3$ explants for both genotypes; $^{**}p = .0048$; mean ± *SD*. Mtmr2 levels were normalized to the β-tubulin signal in the corresponding gel/blot lane. Data were normalized such that the mean value for the wild-type sample was 100. MTMR = myotubularin-related.

the active Mtmr2-like PI 3-phosphatase to specific cortical and vesicular membranes (Jean et al., 2012). With these findings in mind, Mtmr2 might be viewed as biochemically downstream of the catalytically inactive Mtmr13. Thus, if myelin outfoldings in *Mtmr13*$^{-/-}$ Schwann cells are triggered by elevated PI3P or PI(3,5)P_2, reducing the levels of these phosphoinositides might suppress the formation of these abnormal membrane structures. To test this hypothesis, we generated a lentivirus that expresses EGFP-MTMR2 and used this tool to introduce the protein into *Mtmr13*$^{-/-}$ SC-DRG explant cultures.

When introduced into SC-DRG explants, the EGFP-MTMR2 protein was localized to the Schwann cell cytoplasm and was excluded from the nucleus (Figure 6 (e)), consistent with earlier reports on the localization of endogenous Mtmr2 in Schwann cells (Previtali et al., 2003; Ng et al., 2013). In contrast, a lentivirus-expressed EGFP control protein was present in both the nucleus and the cytoplasm of Schwann cells (Figure 6(d)). Virally expressed EGFP and EGFP-MTMR2 were also present in the axons, neuronal soma, and fibroblasts of explant cultures. When explants were virally transduced using the same MOI, EGFP invariably accumulated to much higher levels than did EGFP-MTMR2 (Figure 6(b) and (C)), consistent with the very long half-life of the GFP protein in mammalian cells (~26 h; Corish and Tyler-Smith, 1999). Using an MOI at which greater than 90% of all

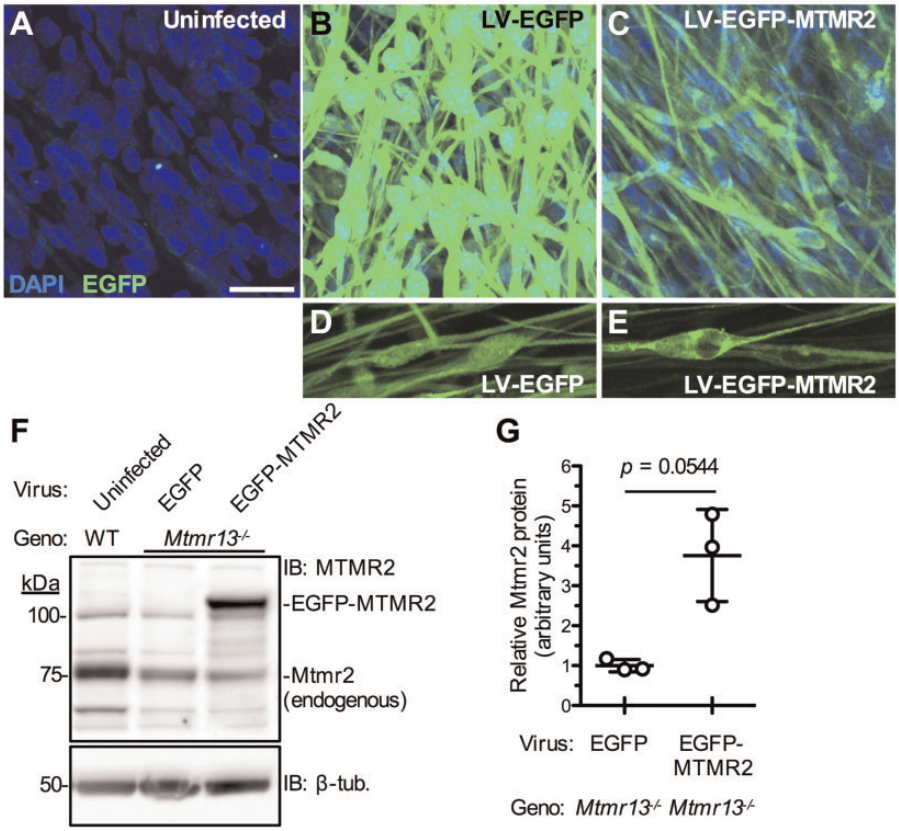

Figure 6. Expression of EGFP-MTMR2 in myelinating DRG explants at levels similar to those of endogenous Mtmr2. (a–c) *Mtmr13*$^{-/-}$ SC-DRG explants were infected with LV-encoding EGFP or EGFP-MTMR2, or left uninfected (a). Infection was on Day 5 and carried out at an MOI of 20. More than 90% of the Schwann cells in an explant were infected with EGFP or EGFP-MTMR2 under these conditions. At 21 days, explants were analyzed for EGFP fluorescence (*green*); nuclei were stained with DAPI (*blue*). Despite similar viral transduction rates, EGFP fluorescence was significantly brighter than EGFP-MTMR2. (d and e) Higher magnification images of explants similar to (b) and (c), respectively (MOI = 15). While EGFP is observed in both the nucleus and cytoplasm of Schwann cells (d), EGFP-MTMR2 is excluded from the nucleus (e). Scale bar: 20 μm (a–c), 15.7 μm (d and e). (f) Immunoblot analysis of endogenous Mtmr2 and EGFP-MTMR2 protein levels in SC-DRG explants after lentivirus infection (MOI = 15; 20 μg of protein per lane). (g) Quantitation of relative Mtmr2 and EGFP-MTMR2 protein levels via immunoblotting (IB) with an anti-MTMR2 antibody. For the LV-EGFP-infected and LV-EGFP-MTMR2-infected explants, the bar graph reports the levels of the endogenous Mtmr2 protein and the EGFP-MTMR2 protein, respectively. Relative Mtmr2/MTMR2 protein: 1.000 ± 0.1532 for LV-EGFP infected versus 3.757 ± 1.152 LV-EGFP-MTMR2 infected (arbitrary units); $p = .0544$; $n = 3$ explants for each condition; mean ± *SD*. Mtmr2 levels were normalized to the β-tubulin signal in the corresponding gel/blot lane. Data were normalized such that the mean value for the wild-type sample was 1. Geno = genotype; MTMR = myotubularin-related; EGFP = enhanced green fluorescent protein; DAPI = 4′,6-diamidino-2-phenylindole; LV = lentiviruses.

Schwann cells were infected, we found that EGFP-MTMR2 was expressed at a level about 3 times that of the endogenous Mtmr2 in *Mtmr13*$^{-/-}$ SC-DRG (Figure 6 (f) and (g) and Supplemental Figure S1), and about twice the level of endogenous Mtmr2 in wild-type SC-DRG explants (Figure 6(f)). Thus, we established conditions whereby MTMR2 protein expression is restored to a level moderately higher than that of the wild type in nearly all the cells present in a given explant culture.

Lentiviral expression of EGFP-MTMR2 in *Mtmr13*$^{-/-}$ SC-DRG explants reduced the prevalence of myelin outfoldings by about 25% (Figure 7(a) to (e)), suggesting that, by reducing the levels of PI3P and/or PI(3,5)P_2, the exogenous MTMR2 protein prevented the formation of myelin outfoldings to a moderate degree. We also noted that MTMR2 overexpression in *Mtmr13*$^{-/-}$ SC-DRGs suppressed myelination globally (Figure 7(f) to (i)). Both the number of myelin segments per unit area and the average length of segments were significantly decreased (Figure 7(j) and (k)). Thus, in the context of relatively modest overexpression, exogenous MTMR2 reduced the efficiency of myelination, presumably by lowering the levels of the MTMR2 lipid substrates PI3P and PI(3,5)P_2.

As described earlier, the overexpression of EGFP-MTMR2 in *Mtmr13*$^{-/-}$ SC-DRG explants caused only a moderate reduction in the prevalence of myelin outfoldings. Thus, much of the *Mtmr13*$^{-/-}$ phenotype persists even when Mtmr2 is brought back to at least wild-type levels. This finding suggests that the most critical function of MTMR13 may not be the stabilization of MTMR2 (and concomitant enhancement of PI 3-phosphatase activity). We sought to further probe the relationship between PI3P/PI(3,5)P_2 and the myelin abnormalities associated with the loss of MTMR13. Given that the pathology associated with Mtmr13 loss appears to be manifested only during myelination (Tersar et al., 2007; Robinson et al., 2008; Ng et al., 2013), and that myelinating Schwann cells represent a relatively minor component of the total cellular material in a cultured DRG explant, we chose to take an *in vivo* genetic approach to manipulating phosphoinositide levels.

Elimination of PI 3-Kinase Isoforms That Generate PI3P Does Not Alter Myelin Abnormalities Associated With Loss of the Mtmr13 Pseudophosphatase

It remains unclear how the balance of PI 3-kinase and 3-phosphatase activities maintains appropriate levels of PI3P, particularly in specialized mammalian cell types (Figure 1(a); Raiborg et al., 2013). It is predicted that CMT4B-causing, loss-of-function mutations in *MTMR13* or *MTMR2* may lead to pathogenic elevation of PI3P and PI(3,5)P_2 in Schwann cells (Cao et al., 2008; Figure 1(a)). Indeed, it has been demonstrated that genetic and pharmacological manipulations which lower PI(3,5)P_2 levels reduce the prevalence myelin outfoldings in *Mtmr2*$^{-/-}$ nerves and explant cultures (Vaccari et al., 2011). We therefore investigated whether genetic mutations predicted to lower PI3P and PI(3,5)P_2 levels in *Mtmr13*$^{-/-}$ Schwann cells would reduce the prevalence myelin outfoldings in an *in vivo* model of CMT4B2, presumably by normalizing endosomal trafficking. To do so, we generated *Mtmr13*$^{-/-}$ *Vps34*^{SCKO} mice, in which Vps34 is selectively deleted in Schwann cells, and compared the nerves of these animals to those of *Mtmr13*$^{-/-}$ mice. Schwann cell-specific deletion of Vps34 had no significant impact on the prevalence of myelin outfoldings in *Mtmr13*$^{-/-}$ sciatic nerves (Figure 8(a) and (b)). This finding suggests that, in Schwann cells, Vps34 is not responsible for generating a pool of PI3P that is critically dephosphorylated by the Mtmr2-Mtmr13 phosphatase complex.

Schwann cell-specific deletion of *Vps34* leads to a significant arrest of myelination beginning at postnatal Day 7 (P7), as well as abnormalities in endosomal-lysosomal trafficking (Figure 8(a) and (c); Logan et al., 2017). Those axons which are myelinated in *Vps34*^{SCKO} mouse nerves are invariably hypomyelinated. *Vps34*^{SCKO} nerves also show abnormal regulation of the erythroblastosis oncogene B (ErbB2)/3 receptor tyrosine kinases, critical components of the promyelinating signaling program in Schwann cells (Logan et al., 2017). ErbB2/3 are known to transit through early endosomes (Sorkin and Goh, 2009), consistent with their altered regulation in the absence of Schwann cell Vps34 (Logan et al., 2017).

Vps34 has been shown to be responsible for producing about 65% of the total PI3P present in mammalian cells (Devereaux et al., 2013; Ikonomov et al., 2015; Figure 1 (a)). Deletion of *Vps34* also lowers PI(3,5)P_2 levels by about 65%, as this lipid is thought to be largely derived from PI3P (Ikonomov et al., 2015; Figure 1(a)). Thus, in *Mtmr13*$^{-/-}$ *Vps34*^{SCKO} Schwann cells, a likely substantial suppression of PI3P and PI(3,5)P_2 levels (caused by loss of Vps34) triggers endosomal trafficking defects that prevent or inhibit myelination after P7 (Figure 8(a)). Under these conditions, the myelin outfoldings triggered by Mtmr13-deficiency form unabated. This *in vivo* finding strongly suggests that elevated PI3P or PI(3,5)P_2 levels are not a significant trigger of myelin outfoldings in *Mtmr13*$^{-/-}$ Schwann cells.

In addition to Vps34, the class II PI 3-kinases are candidates for the enzymes that generate PI3P in Schwann cells (Maffucci and Falasca, 2014). Moreover, there are a number of examples where Class II PI3Ks generate the pools of PI3P targeted by MTMR phosphatases (Srivastava et al., 2009; Velichkova et al., 2010; Razidlo

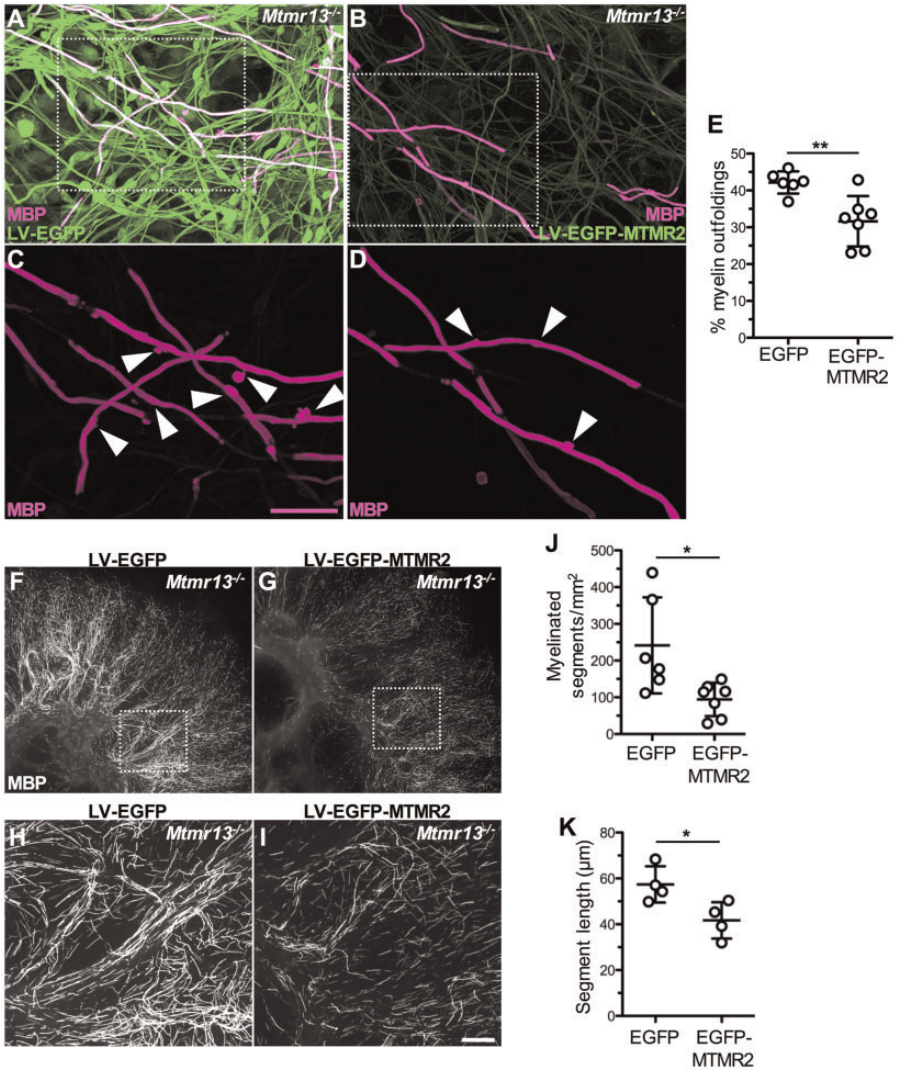

Figure 7. Expression of MTMR2 reduces CMT4B2-like myelin outfoldings in *Mtmr13*$^{-/-}$ DRG explants. (a and b) *Mtmr13*$^{-/-}$ SC-DRG explants were infected with lentiviruses (LV) encoding EGFP or EGFP-MTMR2. Infection was on Day 5 and carried out at an MOI of 20. More than 90% of Schwann cells in an explant were infected with EGFP or EGFP-MTMR2 under these conditions. At 21 days, explants were analyzed for EGFP fluorescence (*green*) and MBP immunofluorescence (*magenta*). White color indicates colocalization of green and magenta. Despite similar viral transduction rates, EGFP fluorescence was invariably significantly brighter than that of EGFP-MTMR2. (c and d) Higher magnification images of the indicated portions of (a) and (b), respectively. Myelin outfoldings (*white arrowheads*) are reduced in number in explants expressing EGFP-MTMR2. (e) Percentage of myelin segments containing one or more outfoldings: 42.16 ± 3.019% versus 31.62 ± 6.851% for LV-EGFP and LV-EGFP-MTMR2 infected, respectively. $^{**}p = .0052$; $n = 6$ and 7 for LV-EGFP and LV-EGFP-MTMR2 infected explants, respectively; mean ± *SD*. An average of 502 myelin segments per explant/coverslip were evaluated for the presence of outfoldings (the median value was 344 myelin segments evaluated per explant/coverslip). Magenta scale bar: 50 μm (a and b), 27 μm (c and d). (f and g) Moderate overexpression of MTMR2 suppresses myelination in *Mtmr13*$^{-/-}$ DRG explants. At 21 days, the extent of myelination was assessed via MBP immunofluorescence (*white*). (h and i) Higher magnification images of the indicated portions of F and G, respectively. (j) Density of myelinated segments: 241.5 ± 130.8 versus 94.38 ± 45.59 segments/mm^2 for LV-EGFP and LV-EGFP-MTMR2 infected, respectively. $^{*}p = .0395$; $n = 6$ and 7 for LV-EGFP and LV-EGFP-MTMR2 infected explants, respectively; mean ± *SD*. In assessing myelin density, an average of 502 myelin segments were counted per explant/coverslip (the median value was 344 myelin segments counted per explant/coverslip). (k) Average length of myelinated segments: 57.40 ± 7.906 μm versus 41.69 ± 7.924 μm for LV-EGFP and LV-EGFP-MTMR2 infected, respectively. $^{*}p = 0.0309$; $n = 4$ for LV-EGFP and LV-EGFP-MTMR2 infected explants; mean ± *SD*. Myelin segment length was determined for 100 segments from each explant/coverslip. White scale bar: 1 mm (f and g), 266 μm (h and i). MTMR = myotubularin-related; EGFP = enhanced green fluorescent protein; LV = lentiviruses; MBP = myelin basic protein.

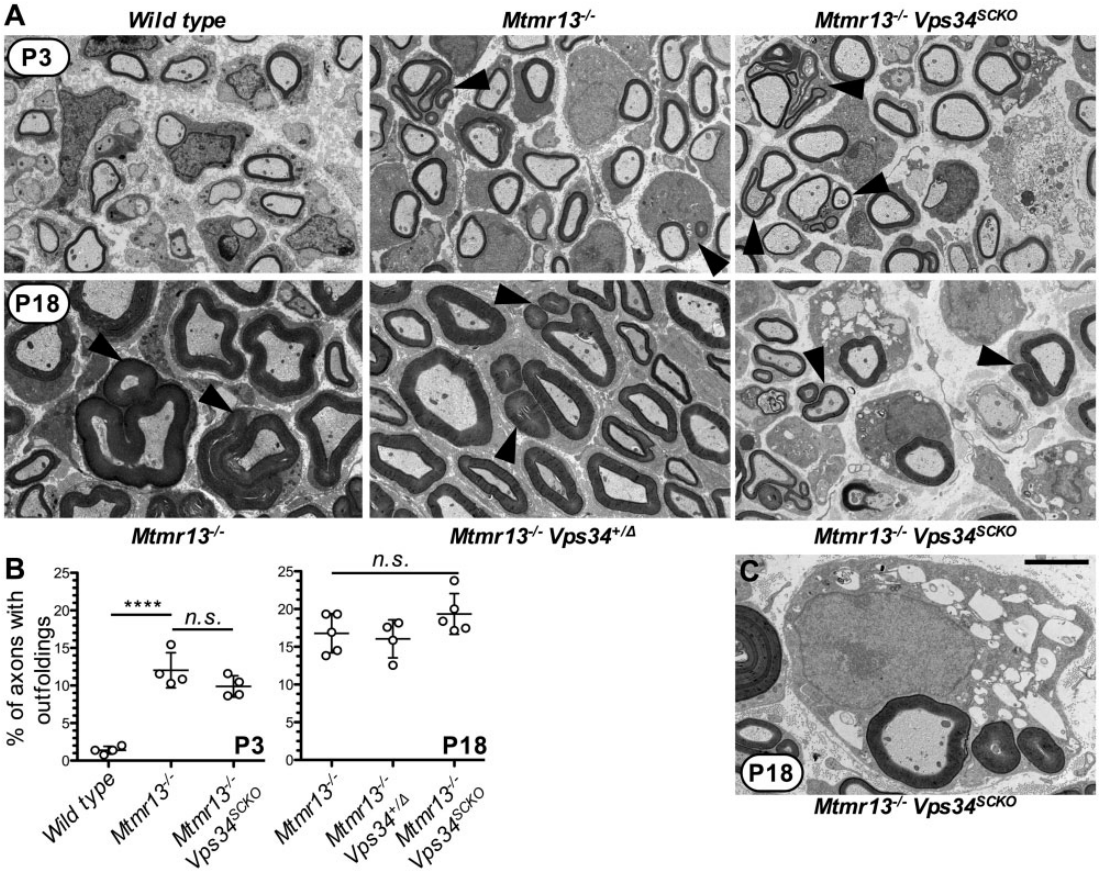

Figure 8. Schwann cell-specific deletion of *Vps34* does not alter the myelin abnormalities caused by Mtmr13-deficiency. (a) EM morphology of midsciatic nerves from P3 wild-type, *Mtmr13*$^{-/-}$, and *Mtmr13*$^{-/-}$ *Vps34*^{SCKO} mice (*upper panels*) and P18 *Mtmr13*$^{-/-}$, *Mtmr13*$^{-/-}$ *Vps34*$^{+/\Delta}$, *and Mtmr13*$^{-/-}$ *Vps34*^{SCKO} mice (*lower panels*). Myelin outfoldings (*arrowheads*) are observed in *Mtmr13*$^{-/-}$, *Mtmr13*$^{-/-}$ *Vps34*$^{+/\Delta}$, *Mtmr13*$^{-/-}$ *Vps34*^{SCKO} nerves. (b) Quantification of myelin outfoldings observed in (a). The percentage of myelinated fibers containing outfoldings is presented as mean $\pm$ *SD*. At P3, the frequency of myelin outfoldings was not significantly different between *Mtmr13*$^{-/-}$ and *Mtmr13*$^{-/-}$ *Vps34*^{SCKO} nerves (12.04 $\pm$ 2.34% for *Mtmr13*$^{-/-}$ versus 9.88 $\pm$ 1.41% for *Mtmr13*$^{-/-}$ *Vps34*^{SCKO}; $p > .05$ using a one-way ANOVA with Sidak's multiple comparisons test to evaluate significance; $n = 4$ mice of each genotype; ****$p \leq .0001$). Likewise, at P18, the frequency of myelin outfoldings was not significantly different between *Mtmr13*$^{-/-}$, *Mtmr13*$^{-/-}$ *Vps34*$^{+/\Delta}$, or *Mtmr13*$^{-/-}$ *Vps34*^{SCKO} nerves (16.78 $\pm$ 2.594% for *Mtmr13*$^{-/-}$ versus 16.05 $\pm$ 2.521% for *Mtmr13*$^{-/-}$ *Vps34*$^{+/\Delta}$ versus 19.35 $\pm$ 2.697% for *Mtmr13*$^{-/-}$ *Vps34*^{SCKO}; $p = .1739$; $n = 5$ for *Mtmr13*$^{-/-}$ mice and *Mtmr13*$^{-/-}$ *Vps34*^{SCKO} mice; $n = 4$ for *Mtmr13*$^{-/-}$ *Vps34*$^{+/\Delta}$ mice). A one-way ANOVA with Tukey's Multiple Comparison Test was used to evaluate the significance. (c) A higher magnification EM image of an *Mtmr13*$^{-/-}$ *Vps34*^{SCKO} Schwann cell containing both cytoplasmic vacuoles and myelin outfoldings (analyzed at P18). Scale bar: 4 μm (a), 2.5 μm (c). MTMR = myotubularin-related. Vps = Vacuolar protein sorting; MTMR = myotubularin-related.

et al., 2011 ; Jean et al., 2012; Kutchukian et al., 2016; Sabha et al., 2016; Figure 1(a)). Therefore, we considered whether PI3K-C2β might enzymatically oppose the MTMR2-MTMR13 phosphatase complex in the regulation of PI3P. To test this, we generated *Mtmr13*$^{-/-}$ *Pik3c2β*$^{-/-}$ double mutant mice and compared the nerve pathology of these animals to that of *Mtmr13*$^{-/-}$ mice. We found that the additional deletion of PI3K-C2β did not significantly reduce the prevalence of myelin outfoldings in *Mtmr13*$^{-/-}$ nerves (Figure 9). In summary, genetic elimination of Vps34 or PI3K-C2β, two manipulations known to lower PI3P and PI(3,5)P_2 levels (Devereaux et al., 2013; Ikonomov et al., 2015), has no impact on the prevalence of myelin outfoldings in *Mtmr13*$^{-/-}$ mice.

Discussion

Mtmr13 Provides a Unique Function That Cannot be Overcome by Overexpressing Its Catalytically Active Binding Partner, Mtmr2

MTMR13 is a 208-kDa, multidomain scaffold protein that contains an inactive version of a PI 3-phosphatase domain (Senderek et al., 2003; Robinson and Dixon, 2005). MTMR13 contains a differentially expressed in normal versus neoplastic (DENN) domain, which activates Rab GTPases by catalyzing guanosine diphosphate for guanosine triphosphate (GTP) exchange in these regulators of membrane trafficking (Yoshimura et al., 2010;

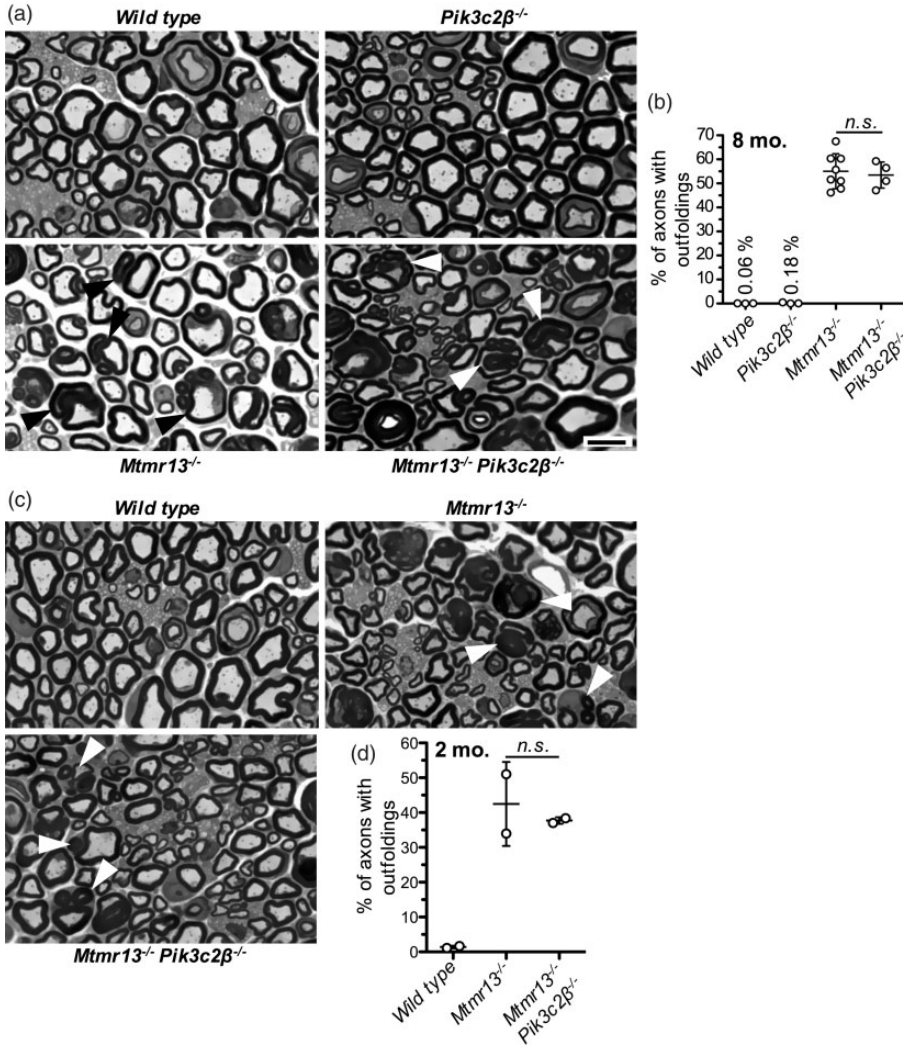

Figure 9. Loss of PI 3-kinase C2β does not affect peripheral nerve myelination or alter the myelin abnormalities caused by Mtmr13-deficiency. (a) Toluidine blue stained cross-sections of the midsciatic nerve from 8-month-old wild-type, *Pik3c2β*$^{-/-}$, *Mtmr13*$^{-/-}$, and *Mtmr13*$^{-/-}$ *Pik3c2β*$^{-/-}$ mice. Peripheral nerve myelination and axonal integrity in *Pik3c2β*$^{-/-}$ nerves was similar to wild types, whereas nerves from *Mtmr13*$^{-/-}$ and *Mtmr13*$^{-/-}$ *Pik3c2β*$^{-/-}$ mice contain numerous myelin outfoldings (*black or white arrowheads*). (b) Quantification of myelin outfoldings observed in (a). At 8 months, the frequency of myelin outfoldings was not significantly different between *Mtmr13*$^{-/-}$ and *Mtmr13*$^{-/-}$ *Pik3c2β*$^{-/-}$ nerves (55.1 ± 7.28% for *Mtmr13*$^{-/-}$ versus 53.5 ± 5.42% for *Mtmr13*$^{-/-}$ *Pik3c2β*$^{-/-}$; $p = .71$; $n = 4$–8 mice per genotype). (c) Toluidine blue stained cross-sections of the midsciatic nerve from 2-month-old wild-type, *Mtmr13*$^{-/-}$, and *Mtmr13*$^{-/-}$ *Pik3c2β*$^{-/-}$ mice. (d) Quantification of myelin outfoldings observed in (c). The frequency of myelin outfoldings was not significantly different between *Mtmr13*$^{-/-}$ and *Mtmr13*$^{-/-}$ *Pik3c2β*$^{-/-}$ nerves (42.5 ± 12.05% for *Mtmr13*$^{-/-}$ versus 37.7 ± 0.946% for *Mtmr13*$^{-/-}$ *Pik3c2β*$^{-/-}$; $p = .63$; $n = 2$ mice per genotype; mean ± *SD*; *n.s.*, not significant). Scale bar: 6 μm.
MTMR = myotubularin-related.

Jean et al., 2012; Figure 1). MTMR13 and the catalytically active PI 3-phosphatase MTMR2 form a stable complex thought to function by dephosphorylating PI3P and PI(3,5)P_2 on endosomal-lysosomal membranes (Robinson and Dixon, 2005; Berger et al., 2006; Jean et al., 2012; Ng et al., 2013).

A number of findings support a specific but limited role of MTMR13 in endosomal-lysosomal trafficking, rather than a strict requirement for the protein for endocytosis or lysosome biogenesis (Ng et al., 2013; Jean et al., 2015). In *Drosophila* macrophages, orthologs of MTMR13, MTMR2, and Rab21 function together in a complex which promotes the recycling of membrane proteins from endosomes. In this context, endosomal recycling requires both the GDP or GTP exchange factor activity of the DENN domain and the PI 3-phosphatase activity of Mtm (Jean et al., 2012). The regulation of endosomal trafficking by SET (domain) binding factor (Sbf)/MTMR13 influences fly macrophage cell shape by controlling cortical actin remodeling (Jean et al., 2012).

The coordinated action of MTMR13 and Rab21 on endosomes has also been shown to positively regulate starvation-induced autophagy in HeLa cells (Jean et al., 2015).

How the roles for MTMR13/Sbf in endosomal trafficking, actin dynamics, and autophagy, largely identified in *Drosophila* cells and mammalian cancer cell lines (Jean et al., 2015), relate to the apparently critical function of the protein in myelinating Schwann cells is unclear. The finding that canonical, Atg7-dependent autophagy is dispensable for developmental myelination by Schwann cells (Gomez-Sanchez et al., 2015; Jang et al., 2015), suggests that MTMR13's role in autophagosome-lysosome fusion may not be responsible for the myelin outfoldings associated with CMT4B2.

With an *in vitro* model of CMT4B2 available, we investigated the relationship between the MTMR2-MTMR13 complex and its lipid substrates. Whether the distinctive myelin outfoldings of CMT4B2 (MTMR13-deficiency) are caused by elevated PI3P or PI(3,5)P_2 is unclear. We probed this question by overexpressing MTMR2 in *Mtmr13*$^{-/-}$ SC-DRG explant cultures, a manipulation predicted to reduce PI3P and PI(3,5)P_2 levels. We found that MTMR2 expression reduced the prevalence of myelin outfoldings by about 25%, thus partially suppressing the CMT4B-like phenotype. Our lentiviral expression strategy brought MTMR2 protein levels to about threefold higher than that of endogenous Mtmr2 in *Mtmr13*$^{-/-}$ SC-DRG explants (about 1.5-fold higher than that of endogenous Mtmr2 in wild-type SC-DRG explants). Thus, we have expressed MTMR2 at supraphysiological levels but not at an extreme level of overexpression.

Our findings using myelinating DRG explant cultures suggest that lowering cellular PI3P or PI(3,5)P_2 moderately reduced the formation of myelin outfoldings, which form in the absence of Mtmr13. Thus, although catalytically inactive itself, Mtmr13 may promote the PI 3-phosphatase activity of Mtmr2 during normal myelination. This may be accomplished by physically stabilizing the Mtmr2 protein or recruiting Mtmr2 to endosomal membranes where PI3P and PI(3,5)P_2 are present (Robinson and Dixon, 2005; Jean et al., 2012; Ng et al., 2013). Our findings using explant cultures are consistent with the hypothesis that elevated PI3P or PI(3,5)P_2 contributes to the myelin abnormalities of CMT4B and suggests that, in Schwann cells, MTMR13 acts as a negative regulator of PI3P/PI(3,5)P_2 abundance. A genetic experiment in *Drosophila* also indicated a role of an MTMR13 ortholog as a negative regulator of PI3P (Jean et al., 2012). Analogous studies of Mtmr2 have suggested that elevated PI(3,5)P_2 leads to excessive longitudinal myelin growth and CMT4B-like outfoldings (Vaccari et al., 2011).

To further probe whether elevated PI3P/PI(3,5)P_2 might cause the myelin outfoldings associated with Mtmr13 loss, we performed two *in vivo* genetic experiments. We generated double-knockout mice that lacked both Mtmr13 and one of two specific PI 3-kinases known to generate PI3P (Vps34 or PI3K-C2β; Figure 1; Devereaux et al., 2013; Ikonomov et al., 2015). Intriguingly, we found that neither the Schwann cell-specific deletion of Vps34 nor the global knockout of PI3K-C2β had any significant impact on the prevalence of myelin outfoldings in *Mtmr13*$^{-/-}$ sciatic nerves. Thus, mutations likely to yield substantial reductions of PI3P, and presumably PI(3,5)P_2, did not suppress the hallmark *Mtmr13*$^{-/-}$ phenotype, suggesting that the elevation of these phosphoinositides in Schwann cells does not contribute significantly to myelin outfoldings in models of CMT4B2. This *in vivo* finding might be viewed as somewhat at odds with our result using *Mtmr13*$^{-/-}$ SC-DRG cultures, where heterologous expression of MTMR2 moderately reduced the prevalence of myelin outfoldings (25% reduction). However, it is worth noting that the overexpression of MTMR2 and the deletion of a PI3P-generating PI3K may differ somewhat in terms of impact on the pathway.

As noted earlier, reexpression of MTMR2 in *Mtmr13*$^{-/-}$ SC-DRG explants only partially suppressed the myelin outfolding phenotype, indicating that Mtmr13 may have critical functions other than stabilizing Mtmr2. The activation of Rab GTPases is a formally PI3P/PI(3,5)P_2-independent function of MTMR13 which is likely relevant to our findings. Once activated, Rab GTPases recruit specific effector proteins to membrane microdomains, thereby driving the highly specific membrane fission and fusion events that underpin vectorial membrane transport (Zhen and Stenmark, 2015). In our experiment, even with MTMR2 reexpressed, *Mtmr13*$^{-/-}$ Schwann cells would still lack the Rab GTPase-activating function of MTMR13's highly conserved DENN (GDP or GTP exchange factor) domain. Rab21, Rab28, and Rab27a have each been implicated as targets of the MTMR13 DENN domain; these or other Rab GTPases may be dysregulated in *Mtmr13*$^{-/-}$ SC-DRGs, suggesting a possible cause of altered endosomal-lysosomal trafficking in CMT4B (Yoshimura et al., 2010; Jean et al., 2012; Abuzenadah et al., 2013).

A limitation of this study is that direct measurements of phosphoinositide levels were not carried out. However, previous studies have demonstrated that the PI3Ks Vps34 and PI3K-C2β contribute significantly to the production of PI3P, from which PI(3,5)P_2 is derived (Devereaux et al., 2013; Ikonomov et al., 2015). Moreover, genetic loss of PI3K-C2β isoforms in flies, mice, and mammalian cell lines has previously been shown to robustly suppress phenotypes associated with the loss of MTMR phosphatases and

pseudophosphatases (Srivastava et al., 2009; Velichkova et al., 2010; Razidlo et al., 2011; Jean et al., 2012; Kutchukian et al., 2016; Sabha et al., 2016). These studies support our conclusion that the genetic approaches used herein provide insight into the function of Mtmr13 in myelination.

In summary, while our findings suggest that suppressed Mtmr2 PI 3-phosphatase activity contributes to the formation of myelin outfoldings in *Mtmr13*$^{-/-}$ SC-DRGs, our work simultaneously suggests that additional Mtmr13 functions, such as Rab GTPase activation and the scaffolding of endosomal regulators, are also critical for myelin homeostasis in Schwann cells, particularly *in vivo*.

Balanced Phosphoinositide Kinase and Phosphatase Enzymatic Activity

A group of human genetic diseases are caused by *loss of function* mutations in phosphoinositide phosphatases. These include demyelinating CMT (MTMR2, MTMR5, MTMR13, and FIG4), myotubular myopathy (MTM1), cancer (phosphatase and TENsin homolog), and the multisystem disorders Lowe Syndrome (oculocerebrorenal) and Joubert Syndrome (INPP5E) (Majerus and York, 2009). As such mutations are predicted, and in some cases demonstrated, to lead to elevations in the cellular abundance of the relevant phosphoinositide substrates, understanding how specific pairs of PI kinases and PI phosphatases enzymatically oppose each other is of interest from both a basic science and a therapeutic perspective (Figure 1).

A number of findings have indicated that the inhibition of specific PI3K isoforms can relieve the cellular defects associated with the loss of individual myotubularin PI 3-phosphatases, likely by decreasing the abundance of PI3P or PI(3,5)P_2. For example, the inhibition of Class II PI3Ks has been shown to ameliorate trafficking and signaling defects triggered by the absence of myotubularin phosphatases in *Drosophila* and mammalian cells (Srivastava et al., 2009; Velichkova et al., 2010; Razidlo et al., 2011; Jean et al., 2012). Perhaps most notable, genetic deletion of PI3K-C2β has been demonstrated to restore muscle function to and improve the life span of *Mtm1*-deficient mice (Kutchukian et al., 2016; Sabha et al., 2016). Finally, genetic or pharmacological manipulations known to lower PI(3,5)P_2 levels have been found to decrease the prevalence of myelin outfoldings in nerves or explant cultures from *Mtmr2*$^{-/-}$ mice, suggesting that the pathology of CMT4B1 may be caused by elevated PI(3,5)P_2 (Vaccari et al., 2011). The work we present here, which is focused on the catalytically inactive Mtmr13 protein's role in myelin homeostasis, suggests a less direct correlation between elevated PI3P/PI(3,5)P_2 and phenotypic consequences than has been reported for the catalytically active myotubularin PI 3-phosphatases. However, in light of the aforementioned studies of Mtmr2 function (Vaccari et al., 2011), and given the strong physical association of the Mtmr2 and Mtmr13 proteins (Robinson and Dixon, 2005; Berger et al., 2006), further investigations aimed at identifying the PI kinases responsible for generating those pools of PI3P and PI(3,5)P_2 that are targeted by the MTMR2-MTMR13 phosphatase complex remain warranted.

Endolysosomal Phosphoinositides in Schwann Cell Myelination

We found that the heterologous expression of MTMR2 in *Mtmr13*$^{-/-}$ SC-DRG explants suppresses myelination globally. In these experiments, the exogenously expressed MTMR2 protein is present at a level only about 1.5-fold higher than that of the endogenous protein, making it unlikely that the suppression of myelination results from an extreme overexpression. We propose that modest overexpression of MTMR2 lowers both PI3P and PI(3,5)P_2 levels such that myelination is blunted but not abolished in *Mtmr13*$^{-/-}$ explant cultures. In this context, blunted myelination may be caused by a moderate impairment of endosomal-lysosomal trafficking. Consistent with our assertion, there is *in vivo* evidence indicating that the depletion of PI3P or PI(3,5)P_2 in Schwann cells impairs myelination. First, Schwann cell-specific deletion of *Vps34*, the Class III PI3K thought responsible for generating more than half of cellular PI3P, leads to arrested myelination during early postnatal development (Logan et al., 2017; Figure 1). Moreover, deletion of FIG4, a phosphatase that stimulates PI(3,5)P_2 production by activating the 5-kinase PIKfyve, leads to developmental hypomyelination and demyelination (Vaccari et al., 2015; Figure 1). It is unlikely that the overexpression of MTMR2 lowers PI3P and PI(3,5)P_2 levels as significantly as does the loss of Vps34, a perturbation that severely retards developmental myelination (Logan et al., 2017). It is also worth noting that the loss of the FIG4 phosphatase has been reported to moderately reduce PI(3,5)P_2 levels without altering PI3P levels (Chow et al., 2007; Vaccari et al., 2011; Zolov et al., 2012). Such findings are consistent with the observation that the loss of Vps34 retards myelination much more significantly than does the loss of FIG4 (Vaccari et al., 2015; Logan et al., 2017). In summary, we propose that reducing PI3P or PI(3,5)P_2 abundance to subphysiological levels (via MTMR2 over-expression) retards myelination by interfering with endosomal-lysosomal trafficking, a perturbation that likely impacts the signaling of key transmembrane receptors, such as the ErbB2/3 tyrosine kinase complex (Lee et al., 2017; Logan et al., 2017). Our findings suggest that normal myelination by Schwann cells requires that the level of the PI 3-

phosphatase MTMR2 is maintained within a relatively narrow range.

In summary, we describe here an *in vitro* model of the demyelinating peripheral neuropathy CMT4B2, which is caused by genetic loss of the MTMR13 pseudophosphatase. The model, which consists of DRG explants from *Mtmr13*$^{-/-}$ mice, recapitulates the distinctive myelin outfoldings of the human condition. In addition, myelinating *Mtmr13*$^{-/-}$ explant cultures contain reduced levels of Mtmr2, an active PI 3-phosphatase and key binding partner of Mtmr13. This finding parallels what has been observed in intact sciatic nerves from *Mtmr13*$^{-/-}$ mice and further supports a role for Mtmr13 in stabilizing the Mtmr2 protein. We used both the novel *in vitro* model and *in vivo* mouse models of CMT4B2 to examine how genetic manipulation of PI3P/PI(3,5)P_2 levels might impact formation of the myelin outfoldings, the hallmark feature of MTMR13-deficiency. In aggregate, our findings suggest that the MTMR13 scaffold protein likely has critical functions other than stabilizing MTMR2 to achieve an adequate level of PI 3-phosphatase activity. We anticipate that the *in vitro* model described here will be useful for further investigations of the biochemical and cellular functions of Mtmr13.

Summary

We describe an *in vitro* model of Charcot-Marie-Tooth type 4B2 peripheral neuropathy, which is caused by mutations in *MTMR13*. We validate myelinating cultures from Mtmr13-deficient mice as a model and examine the relationship between Mtmr13 and its binding partner Mtmr2.

Acknowledgments

The authors wish to thank Jonah Chan, James Salzer, and Haesun Kim for expert advice on the culture of DRG and Schwann cells. Deconvolution and spinning disc microscopy and analysis were carried out in the OHSU Advanced Light Microscopy Core at the Jungers Center for Neurosciences Research. The authors wish to thank Aurelie Snyder and Stefanie Kaech Petrie of the Advanced Light Microscopy Core for expert advice. The DeltaVison CoreDV microscope was purchased with a Shared Instrumentation Grant from the National Institutes of Health-National Center for Research Resources (S10-RR023432 to Thomas Keller). The authors wish to thank Robert Kayton, Lisa Dirling Vecchiarelli, Mellissa Williams, and Sue Aicher for assistance with EM, nerve preparation and expert advice. The EM was purchased through a grant from the Murdock Charitable Trust (to Sue Aicher). The E7 (β-tubulin) monoclonal antibody, developed by Dr. Michael Klymkowsky, was obtained from the Developmental Studies Hybridoma Bank, developed under the auspices of the National Institutes of Health-National Institute of Child Health & Human Development, and maintained by The University of Iowa, Department of Biology, Iowa City, IA 52242.

Author Contributions

D. C. R., A. E. M., A. M. L., A. A. L., and F. L. R. designed research; D. C. R., A. E. M., A. M. L., E. J. S., and A. A. L. performed research; D. C. R., A. E. M., A. M. L., A. F. C., E. J. S., and F. L. R. analyzed data; D. C. R. and F. L. R. wrote the article.

Authors' Note

The authors' plan to share materials and manage intellectual property will adhere to the NIH Sharing Policies and Related Guidance on NIH-Funded Research Resources. An example of such is the NIH Policy on Sharing of Model Organisms for Biomedical Research (published in the NIH Guide on May 7, 2004; see notice NOT-OD-04-042). Any replicative reagents (plasmids), sequences of any protein, cDNA or plasmid DNA construct mentioned or used in the article, and any nonreplicative reagents or samples (antibodies, protein extracts), if possible, will be freely available to the broader research community, upon request, either before or immediately after publication. In addition, we will provide detailed experimental procedures upon request. Material transfers will be made with no more restrictive terms than in the Simple Letter Agreement (SLA) or the Uniform Biological Materials Transfer Agreement (UBMTA) and without reach through requirements.

Declaration of Conflicting Interests

The author(s) declared no potential conflicts of interest with respect to the research, authorship, and/or publication of this article.

Funding

The author(s) disclosed receipt of the following financial support for the research, authorship, and/or publication of this article: This work was supported by the National Institutes of Health—National Institute of Neurological Disorders and Stroke grants NS057903 and NS086812 (to F. L. R.) and by the OHSU Neuroscience Imaging Center P30 grant (NS061800; to Sue Aicher), as well as an Oregon Brain Institute Neurobiology of Disease Graduate Fellowship (to A. M. L.), and through the philanthropy of Frank and Julie Jungers. This work was also supported by the National Science Foundation via a Graduate Research Fellowship under Grant No. 2012142196 (to D. C. R).

Supplemental Material

Supplemental material for this article is available online.

References

Abuzenadah, A. M., Zaher, G. F., Dallol, A., Damanhouri, G. A., Chaudhary, A. G., Al-Sayes, F., Gari, M. A., Alzahrani, M., Hindawi, S., & Al-Qahtani, M. H. (2013) Identification of a novel SBF2 missense mutation associated

with a rare case of thrombocytopenia using whole-exome sequencing. *J Thromb Thrombolysis*, *36*, 501–506.

Alonso, A., Sasin, J., Bottini, N., Friedberg, I., Friedberg, I., Osterman, A., Godzik, A., Hunter, T., Dixon, J., & Mustelin, T. (2004). Protein tyrosine phosphatases in the human genome. *Cell*, *117*, 699–711.

Azzedine, H., Bolino, A., Taieb, T., Birouk, N., Di Duca, M., Bouhouche, A., Benamou, S., Mrabet, A., Hammadouche, T., Chkili, T., Gouider, R., Ravazzolo, R., Brice, A., Laporte, J., LeGuern, E. (2003). Mutations in MTMR13, a new pseudophosphatase homologue of MTMR2 and Sbf1, in two families with an autosomal recessive demyelinating form of Charcot-Marie-Tooth disease associated with early-onset glaucoma. *Am J Hum Genet*, *72*, 1141–1153.

Baets, J., De Jonghe, P., & Timmerman, V. (2014). Recent advances in Charcot-Marie-Tooth disease. *Curr Opin Neurol*, *27*, 532–540.

Balice-Gordon, R. J., Bone, L. J., & Scherer, S. S. (1998). Functional gap junctions in the Schwann cell myelin sheath. *J Cell Biol*, *142*, 1095–1104.

Berger, P., Berger, I., Schaffitzel, C., Tersar, K., Volkmer, B., & Suter, U. (2006). Multi-level regulation of myotubularin-related protein-2 phosphatase activity by myotubularin-related protein-13/set-binding factor-2. *Hum Mol Genet*, *15*, 569–579.

Bolino, A., Lonie, L. J., Zimmer, M., Boerkoel, C. F., Takashima, H., Monaco, A. P., & Lupski, J. R. (2001). Denaturing high-performance liquid chromatography of the myotubularin-related 2 gene (MTMR2) in unrelated patients with Charcot-Marie-Tooth disease suggests a low frequency of mutation in inherited neuropathy. *Neurogenetics*, *3*, 107–109.

Bolino, A., Bolis, A., Previtali, S. C., Dina, G., Bussini, S., Dati, G., Amadio, S., Del Carro, U., Mruk, D. D., Feltri, M. L., Cheng, C. Y., Quattrini, A., & Wrabetz, L. (2004). Disruption of Mtmr2 produces CMT4B1-like neuropathy with myelin outfolding and impaired spermatogenesis. *J Cell Biol*, *167*, 711–721.

Bolino, A., Muglia, M., Conforti, F. L., LeGuern, E., Salih, M. A. M., Georgiou, D. M., Christodoulou, K., Hausmanowa-Petrusewicz, I., Mandich, P., Schenone, A., Gambardella, A., Bono, F., Quattrone, A., Devoto, M., & Monaco, A. P. (2000). Charcot-Marie-Tooth type 4B is caused by mutations in the gene encoding myotubularin-related protein-2. *Nat Genet*, *25*, 17–19.

Bolis, A., Coviello, S., Bussini, S., Dina, G., Pardini, C., Previtali, S. C., Malaguti, M., Morana, P., Del Carro, U., Feltri, M. L., Quattrini, A., Wrabetz, L., & Bolino, A. (2005). Loss of Mtmr2 phosphatase in Schwann cells but not in motor neurons causes Charcot-Marie-Tooth type 4B1 neuropathy with myelin outfoldings. *J Neurosci*, *25*, 8567–8577.

Bolis, A., Coviello, S., Visigalli, I., Taveggia, C., Bachi, A., Chishti, A. H., Hanada, T., Quattrini, A., Previtali, S. C., Biffi, A., & Bolino, A. (2009). Dlg1, Sec8, and Mtmr2 regulate membrane homeostasis in Schwann cell myelination. *J Neurosci*, *29*, 8858–8870.

Brennan, K. M., Bai, Y., & Shy, M. E. (2015). Demyelinating CMT–what's known, what's new and what's in store? *Neurosci Lett*, *596*, 14–26.

Cao, C., Backer, J. M., Laporte, J., Bedrick, E. J., & Wandinger-Ness, A. (2008). Sequential actions of myotubularin lipid phosphatases regulate endosomal PI(3)P and growth factor receptor trafficking. *Mol Biol Cell*, *19*, 3334–3346.

Chow, C. Y., Zhang, Y., Dowling, J. J., Jin, N., Adamska, M., Shiga. K., Szigeti, K., Shy, M. E., Li, J., Zhang, X., Lupski, J. R., & Weisman, L. S., & Meisler, M. H. (2007). Mutation of FIG4 causes neurodegeneration in the pale tremor mouse and patients with CMT4J. *Nature*, *448*, 68–72.

Corish, P., & Tyler-Smith, C. (1999). Attenuation of green fluorescent protein half-life in mammalian cells. *Protein Eng*, *12*, 1035–1040.

Devereaux, K., Dall'Armi, C., Alcazar-Roman, A., Ogasawara, Y., Zhou, X., Wang, F., Yamamoto, A., De Camilli, P., & Di Paolo, G. (2013). Regulation of mammalian autophagy by class II and III PI 3-kinases through PI3P synthesis. *PLoS One*, *8*, e76405.

Eldridge, C. F., Bunge, M. B., Bunge, R. P., & Wood, P. M. (1987). Differentiation of axon-related Schwann cells in vitro. I. Ascorbic acid regulates basal lamina assembly and myelin formation. *J Cell Biol*, *105*, 1023–1034.

Follenzi, A., Ailles, L. E., Bakovic, S., Geuna, M., Naldini, L. (2000). Gene transfer by lentiviral vectors is limited by nuclear translocation and rescued by HIV-1 pol sequences. *Nat Genet*, *25*, 217–222.

Fridman, V., & Reilly, M. M. (2015). Inherited neuropathies. *Semin Neurol*, *35*, 407–423.

Gabreels-Festen, A. A., Joosten, E. M., Gabreels, F. J., Stegeman, D. F., Vos, A. J., & Busch, H. F. (1990). Congenital demyelinating motor and sensory neuropathy with focally folded myelin sheaths. *Brain*, *113*, 1629–1643.

Gomez-Sanchez, J. A. et al. (2015) Schwann cell autophagy, myelinophagy, initiates myelin clearance from injured nerves. *J Cell Biol*, *210*, 153–168.

Harada, K., Truong, A. B., Cai, T., & Khavari, P. A. (2005). The class II phosphoinositide 3-kinase C2beta is not essential for epidermal differentiation. *Mol Cell Biol*, *25*, 11122–11130.

Hirano, R., Takashima, H., Umehara, F., Arimura, H., Michizono, K., Okamoto, Y., Nakagawa, M., Boerkoel, C. F., Lupski, J. R., Osame, M., & Arimura, K. (2004). SET binding factor 2 (SBF2) mutation causes CMT4B with juvenile onset glaucoma. *Neurology*, *63*, 577–580.

Houlden, H., King, R. H., Wood, N. W., Thomas, P. K., & Reilly, M. M. (2001). Mutations in the 5' region of the myotubularin-related protein 2 (MTMR2) gene in autosomal recessive hereditary neuropathy with focally folded myelin. *Brain*, *124*, 907–915.

Ikonomov, O. C., Sbrissa, D., Venkatareddy, M., Tisdale, E., Garg, P., & Shisheva, A. (2015). Class III PI 3-kinase is the main source of PtdIns3P substrate and membrane recruitment signal for PIKfyve constitutive function in podocyte endomembrane homeostasis. *Biochim Biophys Acta*, *1853*, 1240–1250.

Jang, S. Y., Shin, Y. K., Park, S. Y., Park, J. Y., Rha, S. H., Kim, J. K., Lee, H. J., & Park, H. T. (2015). Autophagy is involved in the reduction of myelinating Schwann cell

cytoplasm during myelin maturation of the peripheral nerve. *PLoS One*, *10*, e0116624.

Jean, S., Cox, S., Nassari, S., & Kiger, A. A. (2015). Starvation-induced MTMR13 and RAB21 activity regulates VAMP8 to promote autophagosome-lysosome fusion. *EMBO Rep*, *16*, 297–311.

Jean, S., Cox, S., Schmidt, E. J., Robinson, F. L., & Kiger, A. A. (2012). Sbf/MTMR13 coordinates PI(3)P and Rab21 regulation in endocytic control of cellular remodeling. *Mol Biol Cell*, *23*, 2723–2740.

Jerath, N. U., & Shy, M. E. (2015). Hereditary motor and sensory neuropathies: Understanding molecular pathogenesis could lead to future treatment strategies. *Biochim Biophys Acta*, *1852*, 667–678.

Kim, S. A., Vacratsis, P. O., Firestein, R., Cleary, M. L., & Dixon, J. E. (2003). Regulation of myotubularin-related (MTMR)2 phosphatidylinositol phosphatase by MTMR5, a catalytically inactive phosphatase. *Proc Natl Acad Sci U S A*, *100*, 4492–4497.

Kiwaki, T., Umehara, F., Takashima, H., Nakagawa, M., Kamimura, K., Kashio, N., Sakamoto, Y., Unoki, K., Nobuhara, Y., Michizono, K., Watanabe, O., Arimura, H., & Osame, M. (2000). Hereditary motor and sensory neuropathy with myelin folding and juvenile onset glaucoma. *Neurology*, *55*, 392–397.

Kleopa, K. A., & Sargiannidou, I. (2015). Connexins, gap junctions and peripheral neuropathy. *Neurosci Lett*, *596*, 27–32.

Krajewski, K. M., Lewis, R. A., Fuerst, D. R., Turansky, C., Hinderer, S. R., Garbern, J., Kamholz, J., & Shy, M. E. (2000). Neurological dysfunction and axonal degeneration in Charcot-Marie-Tooth disease type 1A. *Brain*, *123*, 1516–1527.

Kutchukian, C., Lo Scrudato, M., Tourneur, Y., Poulard, K., Vignaud, A., Berthier, C., Allard, B., Lawlor, M. W., Buj-Bello, A., & Jacquemond, V. (2016). Phosphatidylinositol 3-kinase inhibition restores Ca2+ release defects and prolongs survival in myotubularin-deficient mice. *Proc Natl Acad Sci U S A*, *113*, 14432–14437.

Lee, S. M., Chin, L. S., & Li, L. (2017). Dysregulation of ErbB receptor trafficking and signaling in demyelinating Charcot-Marie-Tooth Disease. *Mol Neurobiol*, *54*, 87–100.

Lewallen, K. A., Shen, Y. A., De la Torre, A. R., Ng, B. K., Meijer, D., & Chan, J. R. (2011). Assessing the role of the cadherin/catenin complex at the Schwann cell-axon interface and in the initiation of myelination. *J Neurosci*, *31*, 3032–3043.

Logan, A. M., Mammel, A. E., Robinson, D. C., Chin, A. L., Condon, A. F., & Robinson, F. L. (2017). Schwann cell-specific deletion of the endosomal PI 3-kinase Vps34 leads to delayed radial sorting of axons, arrested myelination, and abnormal ErbB2-ErbB3 tyrosine kinase signaling. *Glia*, *65*, 1452–1470.

Maffucci, T., & Falasca, M. (2014). New insight into the intracellular roles of class II phosphoinositide 3-kinases. *Biochem Soc Trans*, *42*, 1378–1382.

Majerus, P. W., & York, J. D. (2009). Phosphoinositide phosphatases and disease. *J Lipid Res*, *50* Suppl, S249–S254.

Maurel, P., Einheber, S., Galinska, J., Thaker, P., Lam, I., Rubin, M. B., Scherer, S. S., Murakami, Y., Gutmann, D. H., & Salzer, J. L. (2007). Nectin-like proteins mediate axon Schwann cell interactions along the internode and are essential for myelination. *J Cell Biol*, *178*, 861–874.

McMurran, C. E., Jones, C. A., Fitzgerald, D. C., & Franklin, R. J. (2016). CNS remyelination and the innate immune system. *Front Cell Dev Biol*, *4*, 38.

Monk, K. R., Feltri, M. L., & Taveggia, C. (2015). New insights on Schwann cell development. *Glia*, *63*, 1376–1393.

Nakhro, K., Park, J. M., Hong, Y. B., Park, J. H., Nam, S. H., Yoon, B. R., Yoo, J. H., Koo, H., Jung, S. C., Kim, H. L., Kim, J. Y., Choi, K. G., Choi, B. O., & Chung, K. W. (2013). SET binding factor 1 (SBF1) mutation causes Charcot-Marie-Tooth disease type 4B3. *Neurology*, *81*, 165–173.

Nave, K. A., & Werner, H. B. (2014). Myelination of the nervous system: Mechanisms and functions. *Annu Rev Cell Dev Biol*, *30*, 503–533.

Ng, A. A., Logan, A. M., Schmidt, E. J., & Robinson, F. L. (2013). The CMT4B disease-causing phosphatases Mtmr2 and Mtmr13 localize to the Schwann cell cytoplasm and endomembrane compartments, where they depend upon each other to achieve wild-type levels of protein expression. *Hum Mol Genet*, *22*, 1493–1506.

Ohnishi, A., Murai, Y., Ikeda, M., Fujita, T., Furuya, H., & Kuroiwa, Y. (1989). Autosomal recessive motor and sensory neuropathy with excessive myelin outfolding. *Muscle Nerve*, *12*, 568–575.

Othmane, K. B., Johnson, E., Menold, M., Graham, F. L., Hamida, M. B., Hasegawa, O., Rogala, A. D., Ohnishi, A., Pericak-Vance, M., Hentati, F., & Vance, J. M. (1999). Identification of a new locus for autosomal recessive Charcot-Marie-Tooth disease with focally folded myelin on chromosome 11p15. *Genomics*, *62*, 344–349.

Pouwels, P. J., Vanderver, A., Bernard, G., Wolf, N. I., Dreha-Kulczewksi, S. F., Deoni, S. C., Bertini, E., Kohlschutter, A., Richardson, W., Ffrench-Constant, C., Kohler, W., Rowitch, D., & Barkovich, A. J. (2014). Hypomyelinating leukodystrophies: Translational research progress and prospects. *Ann Neurol*, *76*, 5–19.

Previtali, S. C., Quattrini, A., & Bolino, A. (2007). Charcot-Marie-Tooth type 4B demyelinating neuropathy: Deciphering the role of MTMR phosphatases. *Expert Rev Mol Med*, *9*, 1–16.

Previtali, S. C., Zerega, B., Sherman, D. L., Brophy, P. J., Dina, G., King, R. H., Salih, M. M., Feltri, L., Quattrini, A., Ravazzolo, R., Wrabetz, L., Monaco, A. P., & Bolino, A. (2003). Myotubularin-related 2 protein phosphatase and neurofilament light chain protein, both mutated in CMT neuropathies, interact in peripheral nerve. *Hum Mol Genet*, *12*, 1713–1723.

Quattrone, A., Gambardella, A., Bono, F., Aguglia, U., Bolino, A., Bruni, A. C., Montesi, M. P., Oliveri, R. L., Sabatelli, M., Tamburrini, O., Valentino, P., Van Broeckhoven, C., & Zappia, M. (1996). Autosomal recessive hereditary motor and sensory neuropathy with focally folded myelin sheaths: Clinical, electrophysiologic, and genetic aspects of a large family. *Neurology*, *46*, 1318–1324.

Raess, M. A., Friant, S., Cowling, B. S., & Laporte, J. (2017). WANTED—Dead or alive: Myotubularins, a large disease-associated protein family. *Adv Biol Regul*, *63*, 49–58.

Raiborg, C., Schink, K. O., & Stenmark, H. (2013). Class III phosphatidylinositol 3-kinase and its catalytic product PtdIns3P in regulation of endocytic membrane traffic. *FEBS J*, *280*, 2730–2742.

Rasband, M. N., & Peles, E. (2015). The nodes of Ranvier: Molecular assembly and maintenance. *Cold Spring Harb Perspect Biol*, *8*, a020495.

Razidlo, G. L., Katafiasz, D., & Taylor, G. S. (2011). Myotubularin regulates Akt-dependent survival signaling via phosphatidylinositol 3-phosphate. *J Biol Chem*, *286*, 20005–20019.

Robinson, F. L., & Dixon, J. E. (2005). The phosphoinositide-3-phosphatase MTMR2 associates with MTMR13, a membrane-associated pseudophosphatase also mutated in type 4B Charcot-Marie-Tooth disease. *J Biol Chem*, *280*, 31699–31707.

Robinson, F. L., Niesman, I. R., Beiswenger, K. K., & Dixon, J. E. (2008). Loss of the inactive myotubularin-related phosphatase Mtmr13 leads to a Charcot-Marie-Tooth 4B2-like peripheral neuropathy in mice. *Proc Natl Acad Sci U S A*, *105*, 4916–4921.

Sabha, N., Volpatti, J. R., Gonorazky, H., Reifler, A., Davidson, A. E., Li, X., Eltayeb, N. M., Dall'Armi, C., Di Paolo, G., Brooks, S. V., Buj-Bello, A., Feldman, E. L., & Dowling, J. J. (2016). PIK3C2B inhibition improves function and prolongs survival in myotubular myopathy animal models. *J Clin Invest*, *126*, 3613–3625.

Salzer, J. L. (2015). Schwann cell myelination. *Cold Spring Harb Perspect Biol*, *7*, a020529.

Scherer, S. S., & Wrabetz, L. (2008). Molecular mechanisms of inherited demyelinating neuropathies. *Glia*, *56*, 1578–1589.

Schink, K. O., Tan, K. W., & Stenmark, H. (2016). Phosphoinositides in control of membrane dynamics. *Annu Rev Cell Dev Biol*, *32*, 143–171.

Senderek, J., Bergmann, C., Weber, S., Ketelsen, U. P., Schorle, H., Rudnik-Schoneborn, S., Buttner, R., Buchheim, E., & Zerres, K. (2003). Mutation of the SBF2 gene, encoding a novel member of the myotubularin family, in Charcot-Marie-Tooth neuropathy type 4B2/11p15. *Hum Mol Genet*, *12*, 349–356.

Skre, H. (1974). Genetic and clinical aspects of Charcot-Marie-Tooth's disease. *Clin Genet*, *6*, 98–118.

Sorkin, A., & Goh, L. K. (2009). Endocytosis and intracellular trafficking of ErbBs. *Exp Cell Res*, *315*, 683–696.

Srivastava, S., Di, L., Zhdanova, O., Li, Z., Vardhana, S., Wan, Q., Yan, Y., Varma, R., Backer, J., Wulff, H., Dustin, M. L., & Skolnik, E. Y. (2009). The class II phosphatidylinositol 3 kinase C2beta is required for the activation of the K+ channel KCa3.1 and CD4 T-cells. *Mol Biol Cell*, *20*, 3783–3791.

Taylor, G. S., Maehama, T., & Dixon, J. E. (2000). Myotubularin, a protein tyrosine phosphatase mutated in myotubular myopathy, dephosphorylates the lipid second messenger, phosphatidylinositol 3-phosphate. *Proc Natl Acad Sci U S A*, *97*, 8910–8915.

Tersar, K., Boentert, M., Berger, P., Bonneick, S., Wessig, C., Toyka, K. V., Young, P., & Suter, U. (2007). Mtmr13/Sbf2-deficient mice: An animal model for CMT4B2. *Hum Mol Genet*, *16*, 2991–3001.

Tiscornia, G., Singer, O., & Verma, I. M. (2006). Production and purification of lentiviral vectors. *Nat Protoc*, *1*, 241–245.

Tonks, N. K. (2013). Protein tyrosine phosphatases–from housekeeping enzymes to master regulators of signal transduction. *FEBS J*, *280*, 346–378.

Vaccari, I., Carbone, A., Previtali, S. C., Mironova, Y. A., Alberizzi, V., Noseda, R., Rivellini, C., Bianchi, F., Del Carro, U., D'Antonio, M., Lenk, G. M., Wrabetz, L., Giger, R. J., Meisler, M. H., & Bolino, A. (2015). Loss of Fig4 in both Schwann cells and motor neurons contributes to CMT4J neuropathy. *Hum Mol Genet*, *24*, 383–396.

Vaccari, I., Dina, G., Tronchere, H., Kaufman, E., Chicanne, G., Cerri, F., Wrabetz, L., Payrastre, B., Quattrini, A., Weisman, L. S., & Meisler, M. H., & Bolino, A. (2011). Genetic interaction between MTMR2 and FIG4 phospholipid phosphatases involved in Charcot-Marie-Tooth neuropathies. *PLoS Genet*, *7*, e1002319.

Velichkova, M., Juan, J., Kadandale, P., Jean, S., Ribeiro, I., Raman, V., Stefan, C., Kiger, A. A. (2010). Drosophila Mtm and class II PI3K coregulate a PI(3)P pool with cortical and endolysosomal functions. *J Cell Biol*, *190*, 407–425.

Walker, D. M., Urbe, S., Dove, S. K., Tenza, D., Raposo, G., & Clague, M. J. (2001). Characterization of MTMR3. an inositol lipid 3-phosphatase with novel substrate specificity. *Curr Biol*, *11*, 1600–1605.

Yoshimura, S., Gerondopoulos, A., Linford, A., Rigden, D. J., & Barr, F. A. (2010). Family-wide characterization of the DENN domain Rab GDP-GTP exchange factors. *J Cell Biol*, *191*, 367–381.

Zhen, Y., & Stenmark, H. (2015). Cellular functions of Rab GTPases at a glance. *J Cell Sci*, *128*, 3171–3176.

Zolov, S. N., Bridges, D., Zhang, Y., Lee, W. W., Riehle, E., Verma, R., Lenk, G. M., Converso-Baran, K., Weide, T., Albin, R. L., Saltiel, A. R., Meisler, M. H., Russell, M. W., & Weisman, L. S. (2012). In vivo, Pikfyve generates PI(3,5) P2, which serves as both a signaling lipid and the major precursor for PI5P. *Proc Natl Acad Sci U S A*, *109*, 17472–17477.